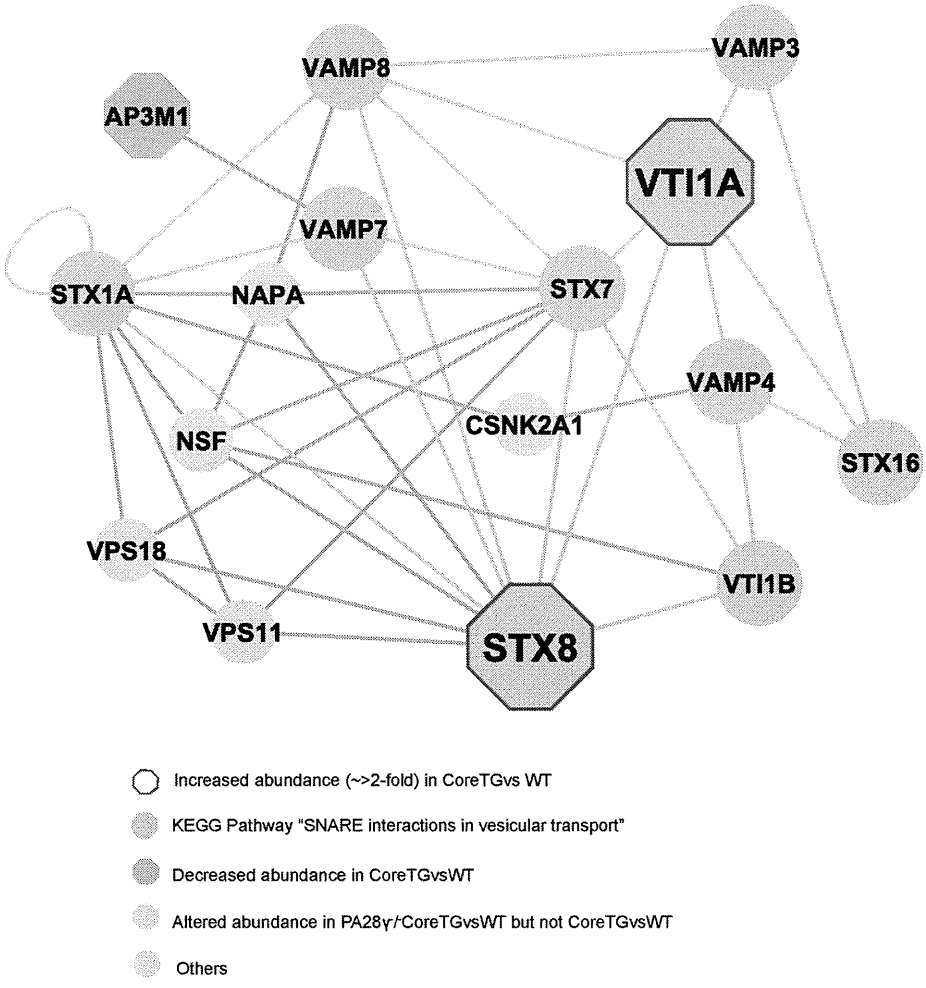

Figure 2. CoreTGvsWT SNARE network. Network illustration of the interactions between the PowerBlot identified differentially expressed proteins in CoreTGvsWT and human proteins mapped to the enriched KEGG pathway "SNARE interactions in vesicular transport". The node sizes differ for better clarity and do not reflect any topological attributes.

mechanism for the involvement of PA28γ in HCV propagation. Potentially, the suppression of PA28γ activity in PA28$\gamma^{-/-}$CoreTG mice may contribute to the overexpression of STX11 (and downregulation of USO1), thereby impairing the trafficking to the cell surface and consequently the release of the infectious HCV particles.

HCV has also been detected in the macrophages of certain infected patients,[64] suggesting that HCV may possibly infect the macrophages *in vivo* and regulate the STX11 (and USO1) expression to modulate the viral release and cytokine secretion.

EPS15 and RABEP1 (KEGG pathway "Endocytosis", $p = 2.08 \times 10^{-22}$) were decreased 2.11- and 2.74-fold, respectively, in PA28$\gamma^{-/-}$CoreTGvsCoreTG (Table 1, Table S5). EPS15 is an adaptor protein associated with the epidermal growth factor (EGF) signaling; it is localized to the clathrin-coated pits and functions in receptor-mediated endocytosis[65,66] and may play an important role in HCV pathogenesis (Table 2).

Immune System and Signal Transduction

HCV infection induces varied active and passive host immune responses such as the recognition of the infecting HCV RNA and proteins by the macrophages and the dendritic cells expressing Toll-like receptors (TLRs) and RIG-I-like receptors (RLRs). These events trigger the production of Type I interferons (IFN-α/β) and inflammatory cytokines in the infected hepatocytes, thereby initiating viral clearance. The ability to impair host immune responses contributes to the HCV persistence in the host.[67−72]

The PowerBlot analysis showed differentially expressed host proteins (IKBKG, MAP2K2, PPP3CA, SHC3, STAT1, TRADD) in PA28$\gamma^{-/-}$CoreTGvsCoreTG and their interacting partners that were mapped to one or more enriched KEGG pathways associated with the immune system (Table S5). IKBKG (IKK Gamma) is an antiapoptotic protein that is essential for NFKB activation and modulates TNF-mediated apoptosis.[73] IKBKG mutations are associated with immune deficiency phenotype (Table S7) and IKBKG may contribute to the activity of the hepatic carcinoma associated protein MAFIP in suppressing the proliferation of the cancer cells.[74] Additionally, specific deletion of IKBKG in the hepatocytes promotes NK-cell dependent liver damage.[75] Taken together, the elevated IKBKG abundance as observed in PA28$\gamma^{-/-}$CoreTGvsCoreTG (1.97-fold; Table 1) may contribute to the lack of HCC progression and reduced liver damage in the PA28$\gamma^{-/-}$CoreTG mice.

PPP3CA, MAP2K2, and SHC3 were mapped to the KEGG pathway "Natural killer cell mediated cytotoxicity" ($p = 1.67 \times 10^{-5}$; Table S5), the components of which function in the host immune response against the cancer cells and cells beset with pathogen infection.[76] PPP3CA levels were increased 12.94-fold,

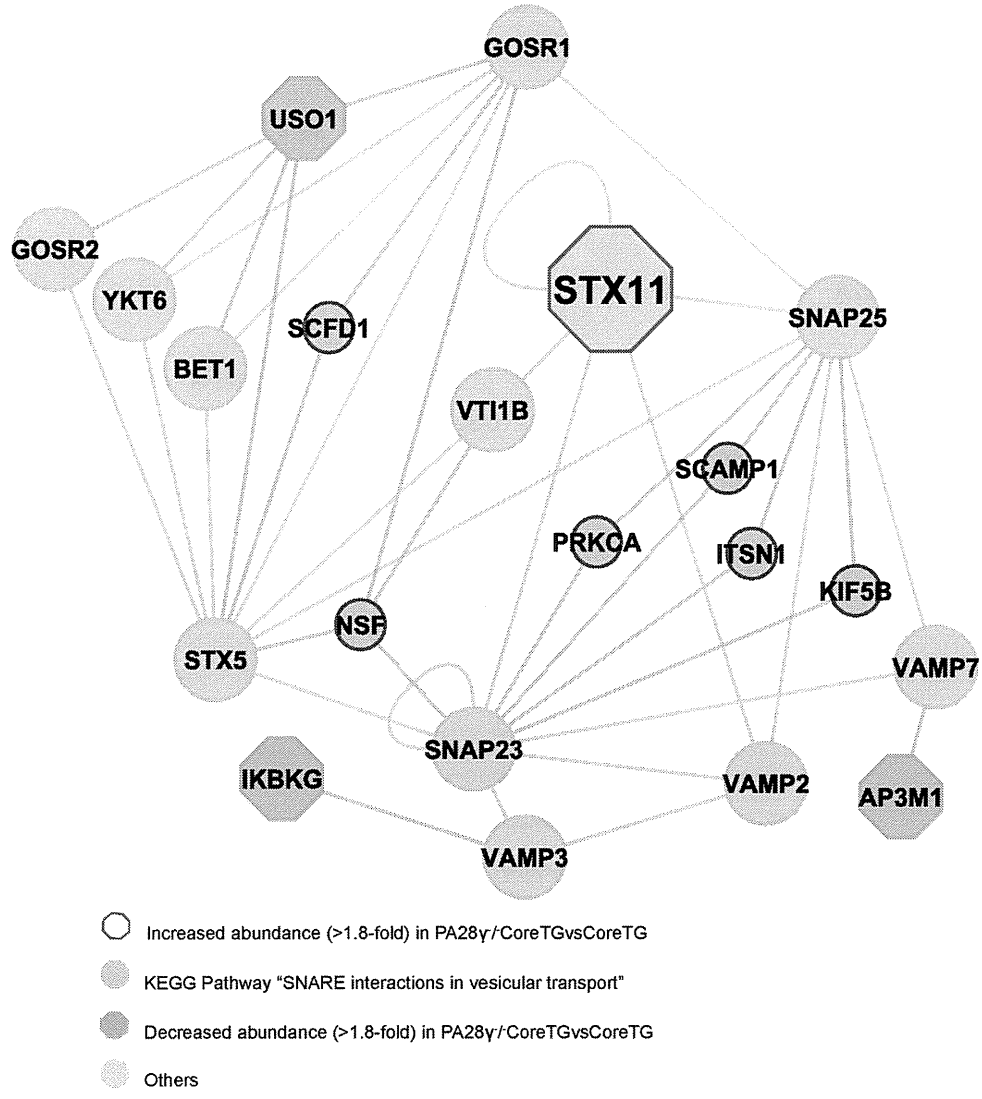

Figure 3. PA28$\gamma^{-/-}$CoreTGvsCoreTG SNARE network. Network illustration of the interactions between the PowerBlot identified differentially expressed proteins in PA28$\gamma^{-/-}$CoreTGvsCoreTG and human proteins mapped to the enriched KEGG pathway "SNARE interactions in vesicular transport". The node sizes differ for better clarity and do not reflect any topological attributes.

while MAP2K2 and SHC3 levels were suppressed 2.35-fold and 1.9-fold, respectively, in PA28$\gamma^{-/-}$CoreTGvsCoreTG (Table 1). These observations together with the increased STX11 abundance are consistent with the enhanced NK-cell mediated cytotoxicity that accompanies the STX11 overexpression.

PPP3CA is a tumor suppressor that negatively modulates the vascular endothelial growth factor (VEGF)-stimulated cell proliferation[77] and is downregulated in some cancerous cells.[78,79] PPP3CA was also mapped to the enriched KEGG pathways "VEGF signaling pathway" ($p = 2.59 \times 10^{-5}$), "MAPK signaling pathway" ($p = 2.37 \times 10^{-16}$) and "Wnt signaling pathway" ($p = 1.048 \times 10^{-10}$; Table S5), which are implicated in the HCV infection and HCC. The 7.55-fold increase in PPP3CA abundance in PA28$\gamma^{-/-}$CoreTGvsCoreTG (Table 1) suggests that increased PPP3CA activity may significantly contribute to the lack of tumorigenesis and HCC progression in PA28$\gamma^{-/-}$CoreTG mice.

MAP2PK2 is a dual specificity MAP kinase that plays a critical role in the mitogen growth factor signal transduction. It is a key regulator of the TNF-α signaling and plays an important role in the tumor progression in certain cancers.[80] Reduced MAP2K2 levels in the hepatocytes are implicated in enhanced apoptosis.[81] Therefore, the 2.66-fold decrease in MAP2K2 protein levels in PA28$\gamma^{-/-}$CoreTGvsCoreTG (Table 1) suggests that decreased MAP2K2 activity may contribute to the lack of HCC progression in PA28$\gamma^{-/-}$CoreTG mice. Our analysis thus identified potentially significant PA28γ-dependent roles of MAP2K2 and PPP3CA in a probable STX11-mediated regulation of NK cell activity in HCV pathogenesis.

MAP2K2, PPP3CA and SHC3 were also associated with the "Insulin signaling pathway" ($p = 5.88 \times 10^{-9}$; Table S5), the disruption of which may contribute to insulin resistance (IR). IR is linked with steatosis, fibrosis progression and poor interferon-α response in HCV infection.[82,83] PA28γ contributes to hyperinsulinemia and IR in the CoreTG mice by impairing the insulin-signaling pathway through the suppression of Insulin receptor substrate 1 (IRS1) phosphorylation and increased tumor necrosis factor alpha (TNF-α) secretion.[12,84] The Powerblot analysis revealed that TRADD, which regulates TNF-α signaling as an antiapoptotic factor[85,86] and possibly functions in HCV pathogenesis (Table 2), was suppressed 2-fold in PA28$\gamma^{-/-}$CoreTGvsWT (Table 1).

Table 3. Summary of Proteins and Pathways Prioritized with TargetMine and Adjusted with the Help of Knowledge-Based Inputs for Experimental Investigation and/or Biomarker Discovery

(a) HCV replication and release

KEGG pathways	*p*-value	proteins[a]	data set[b]	knowledge-based evidence	refs
SNARE interactions in vesicular transport	0.023	VTI1A (+), STX8 (+)	I	regulation of the endosome-based membrane trafficking pathway implicated in HCV release	50, 52, 55
Steroid hormone biosynthesis	0.002	COMT (+)	I	COMT siRNA impairs HCV genotype 1b replication; functions in genotype 2a replication not known	50, 103
SNARE interactions in vesicular transport	0.003	STX11 (+)	III	modulation of specific components of the endosome-based membrane trafficking pathway implicated in HCV release; modulation of cytokine secretion in immune cells	50, 55, 57
Endocytosis	1.03×10^{-18}	CAV1 (+)	I	close homologue CAV2 associated with HCV replication complex; possible role in HCV replication	103

(b) steatosis, fibrosis, and hepatcarcinogenesis in HCV infection

KEGG pathways	*p*-value	proteins[a]	data set[b]	knowledge-based evidence	refs
Insulin signaling pathway	5.72×10^{-12}	AKT1 (−)	I	reduced AKT1 levels and phosophorylation associated with insulin resistance, which contributes to steatosis, fibrosis and HCC	118
Natural killer cell mediated cytotoxicity	1.67×10^{-5}	PPP3CA (+), MAP2K2 (−)	III	PPP3CA is a tumor suppressor with decreased levels in some cancers; PTPN1 is a tumor suppressor and regulates hepatic insulin signaling; decreased MAP2K2 levels in hepatocytes associated with enhanced apoptosis	78, 79, 81
Adherens junction	1.45×10^{-20}	CDH1 (−)	I	decreased CDH1 abundance associated with hepatocarcinogenesis and various cancers	106
Focal adhesion	5.57×10^{-12}	SHC1 (+)	II	loss of SHC1 function associated with tumor metastasis	119
Apoptosis	1.58×10^{-18}	BAX (+), CASP8 (+)	I	BAX interacts with NS5A and contributes to abnormal cytochrome *c* release in HCV infection; CASP8 activated in HCV infection	45, 90, 92, 93
Apoptosis	1.84×10^{-15}	TRADD (−)	III	antiapoptotic factor that forms a ternary complex containing Core, with likely functions in HCV-induced chronic liver disease	117
Chemokine signaling pathway	1.18×10^{-13}	ARRB1 (−)	I	interacts with PKM2, a key enzyme in glycolytic metabolism and cell growth and death in tumor cells	120

[a]+: upregulated. −: downregulated. [b]Data set I: CoreTGvsWT; Data set II: PA28$\gamma^{-/-}$/CoreTGvsWT; Data set III: PA28$\gamma^{-/-}$/CoreTGvsCoreTG.

Cell Adhesion

The Powerblot analysis revealed that host protein CSNK2B, the regulatory (beta) subunit of Casein Kinase II (CK2), was increased 1.88-fold in PA28$\gamma^{-/-}$CoreTGvsCoreTG (1.9-fold in PA28$\gamma^{-/-}$CoreTGvsWT). CK2 phosphorylates NS5A and regulates the production of infectious viral particles[87] and thus HCV pathogenesis (Table 2). CSNK2B was mapped to the enriched KEGG pathways "Adherens junction" ($p = 1.4 \times 10^{-13}$) and "Tight junction" ($p = 4.46 \times 10^{-7}$), some components of which are implicated in HCV entry and infection.[88]

SHC3 and TNR were decreased 1.9- and 4.62-fold, respectively, in PA28$\gamma^{-/-}$CoreTGvsCoreTG and were mapped to the enriched KEGG pathway "Focal adhesion" ($p = 3.56 \times 10^{-12}$; Table 1; Table S5), which regulates cell migration and adhesion to the extracellular matrix. Its deregulation is linked with tumor progression and possibly HCV propagation.[45] Previously, a Core interacting protein ENO1, associated with the focal adhesion, was identified as a novel regulator of HCV replication and release,[22] suggesting that SHC3 and TNR may play important roles in HCV pathogenesis.

Cell Growth and Death

Host cell apoptosis plays a critical role in HCV pathogenesis. The induction of apoptosis in the hepatocytes contributes to cell damage and fibrosis, whereas the induction of apoptosis in the peripheral blood mononuclear cells (PMBC), such as the T-cells, contributes significantly to the impaired immune response and HCV persistence in the host.[89−94] PA28γ is implicated in the cell cycle regulation, cell proliferation, and apoptosis[95−98] and likely plays a critical role in the manipulation of the cell cycle and apoptosis in HCV pathogenesis.

PPP3CA, TRADD, PRKAR2A, and IKBKG, with increased or decreased abundances in PA28$\gamma^{-/-}$CoreTGvsCoreTG, were mapped to KEGG pathway "Apoptosis" ($p = 1.84 \times 10^{-15}$; Table S5). PPP3CA was also mapped to "Oocyte meiosis" ($p = 9.84 \times 10^{-10}$; Table S5), associated with cell division. PPP3CA levels were highly elevated (12.94-fold) in PA28$\gamma^{-/-}$CoreTGvsCoreTG (Table 1), which may contribute to the accelerated cell death and the lack of tumor progression in PA28$\gamma^{-/-}$CoreTG mice.

PRKAR2A levels were decreased 1.88-fold in PA28$\gamma^{-/-}$CoreTGvsCoreTG (Table 1). PRKAR2A codes for a regulatory subunit of the cAMP dependent protein kinase (PKA), an important mediator of the cAMP signal transduction and elevated PRKAR2A expression is associated with an increased proliferation of the rat alveolar cells.[99] The suppression of PRKAR2A activity may therefore contribute to the lack of tumor proliferation in the PA28$\gamma^{-/-}$CoreTG mice.

Prioritization and Validation of the Novel Candidates for Their Role in HCV Replication and Release

Target prioritiszation using TargetMine is a simple process that involves uploading an initial list of candidates (in this instance the proteins in the CoreTGvsWT, PA28$\gamma^{-/-}$CoreTGvsWT, and PA28$\gamma^{-/-}$CoreTGvsCoreTG extended PPI networks) and estimating enriched biological themes associated with the input list.[16] Knowledge-based inputs may then be employed to further screen the proteins mapped to the top ranking significant associations to infer a manageable set of candidates. With the help of TargetMine, we previously investigated the significance of interactions between HCV Core and NS4B proteins and host factors in HCV infection and identified three novel regulators of HCV replication and propagation.[22]

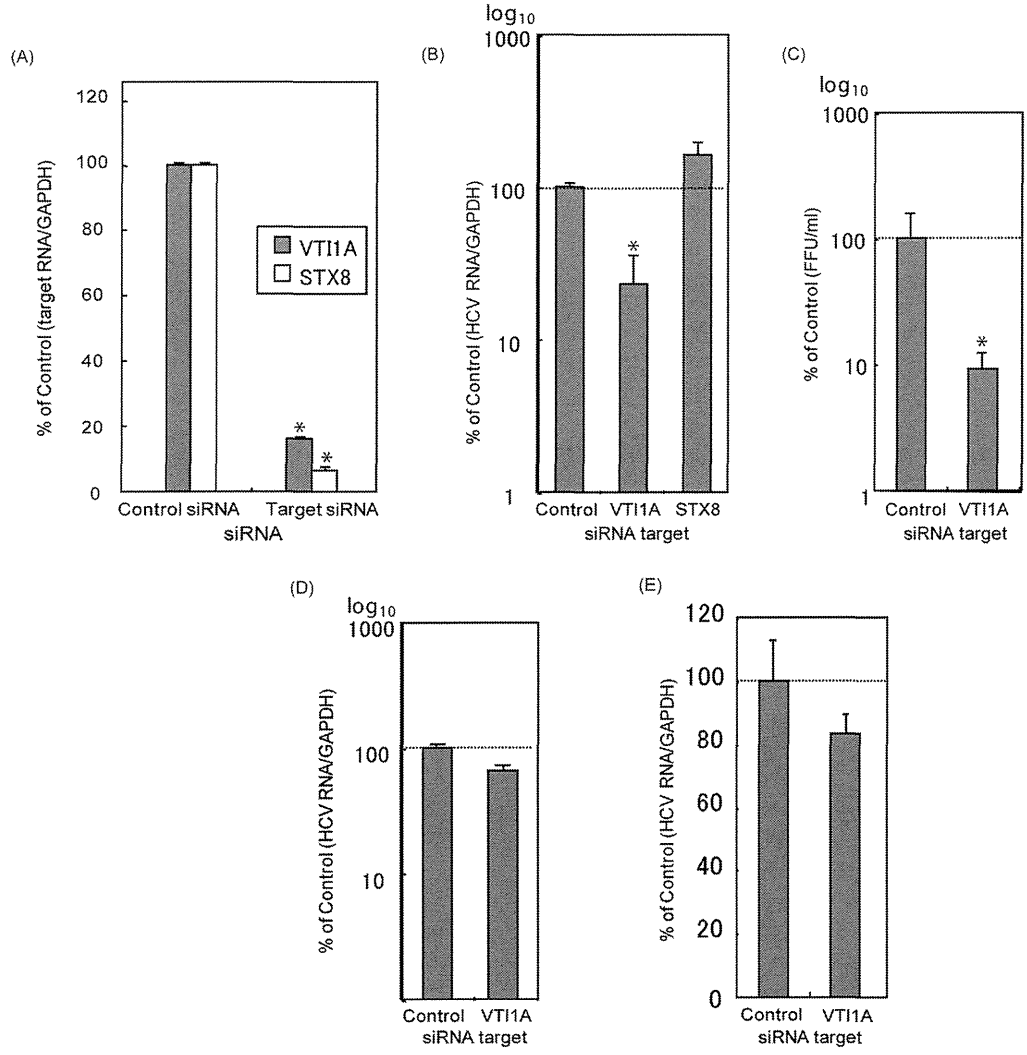

Figure 4. Effects of knockdown of candidate proteins on HCV propagation and replication. Host proteins VTI1A and STX8 were suppressed by RNAi (A) in Huh7OK1 cells infected with HCV JFH1 strain (genotype 2a; B, C, D) and in cells including subgenomic JFH1 replicon (E). The amounts of mRNA of the intracellular host proteins (A) and the supernatant viral RNA (B), viral titer (C), and intracellular viral RNA were estimated (D). The amount of the subgenomic viral RNA was also estimated (E). Each value was represented as percentage of the cells transfected with control siRNA; FFU: focus-forming units; * $p < 0.01$.

Table 3 summarizes the prioritized candidates and pathways, all of which have been discussed above. Traditionally, viral and host proteins associated with the HCV lifecycle (internalization, replication, assembly, and release) have been preferred targets in the anti-HCV studies. The prioritized candidates and pathways in Table 3a fall within this category. In particular, our analysis suggested novel and potentially crucial roles of the host proteins VTI1A and STX8, which were elevated in CoreTG but not in PA28$\gamma^{-/-}$CoreTG, in the replication and/or the release stages of the HCV lifecycle, therefore making these host proteins attractive targets for further investigation.

Because of the lack of a suitable model system for HCV infection, cell-culture-based systems for HCV RNA replication and infectious viral particle production have been extensively exploited to identify potential anti-HCV drug targets.[5,7−9] To further explore the roles of selected candidates in the HCV life cycle, we performed cellular assays to assess the impact of VTI1A and STX8 siRNA knockdowns on HCV replication and release. Since the HCV-production systems using the HCV JFH1 infectious strain (genotype 2a) isolates alone are capable of both efficient replication and the production of the infectious HCV particles,[33,100] JFH1 was used to infect the Huh7OK1 cell line 24 h after transfection with each siRNA (see Materials and Methods). The infected cells were harvested after 72 h post-infection and the expression of each host protein was assessed by qRT-PCR (Figure 4A). Supernatant viral RNA and the viral titer were significantly decreased by the knockdown of VTI1A but were unaffected by the STX8 knockdown (Figure 4B,C). However, VTI1A and STX8A knockdowns had no effect on the intracellular viral RNA levels in the HCV infected cells (Figure 4D) or replicon cells derived from JFH1 strain (Figure 4E) or replicon cells derived from the Con1 (genotype 1b) strain (data not shown). These observations suggest that VTI1A regulates HCV propagation but not HCV replication.

The standard therapy of PEGylated interferon-α plus rebavirin treatment often results in severe side effects such as depression, flu-like symptoms, anemia, and fatigue that force the treatment to discontinue in affected patients, thus necessitating improved and combinatorial treatment strategies.[101,102] The genetic variability of HCV has led to increasing drug resistance. Thus, antivirals that target host proteins critical to viral pathogenesis, with a lower rate of mutation and

preferably with minimal adverse side effects, may provide attractive alternatives to HCV protein targets. VTI1A-deficient (knockout) mice are viable and fertile,[55] suggesting that the suppression of VTI1A activity may not have significantly undesirable side effects.

Inhibition of COMT (which was increased 2.71- and 2.96-fold in CoreTGvsWT and PA28$\gamma^{-/-}$CoreTG, respectively; Table 1) activity via siRNA knockdown was previously shown to result in a decreased HCV replication in cells infected with the Con1 strain.[103] To investigate other possible aspects (such as genotype specificity) of COMT function in the HCV life cycle, we assessed the impact of the COMT siRNA knockdown on HCV replication and release. COMT knockdown, however, had no effect on HCV propagation or replication in the cells including full length or subgenomic replicons derived from JFH1 or Con1 strains (data not shown). The discrepancy between our observations and those of Chan et al.[103] may be explained by the differences in the methodologies. We employed a transient transfection method to knockdown the selected targets to assess their roles in HCV replication and release, whereas Chan et al. employed a lentiviral expressing system for their experiments. Lentiviral mediated siRNA delivery is known to result in a persistent knockdown of gene expression,[104] and a persistent knockdown of COMT expression may be necessary to inhibit HCV replication *in vitro*.

That we were able to experimentally validate one of the three genes selected for experimental characterization reinforces the strengths of the elaborate PPI network-based approach to identify and prioritize suitable targets for experimental and therapeutic investigation.

CONCLUSIONS

By analyzing high-throughput proteomics data from transgenic mice expressing HCV Core protein in the liver (an *in vivo* model of HCV pathogenesis) with or without the knockout of the proteasome activator PA28γ, we highlighted the cellular responses to HCV infection *in vivo* and obtained further insights into the role of PA28γ in HCV infection.

We investigated the network context of the changes in the protein abundances by mapping them onto the human interactome with the help of the TargetMine data warehouse. The differentially expressed proteins that were integrated with the human interactome were observed to participate in compact and well connected cellular networks reflecting the ability of HCV to rapidly and efficiently react to the host responses to HCV infection. A functional analysis of the PPI networks highlighted the cellular pathways associated with vesicular transport, immune system, cellular adhesion, cell growth, and cell death among others that were most prominently influenced by Core and PA28γ in HCV infection. We also confirmed the previous observations that host factors such as AKT1, BAX, CASP8 CDH1, COMT, MCM2, PTPN11, and RB1 showed increased or decreased abundances in HCV infection. However, to the best of our knowledge, the precise molecular mechanisms of these factors' involvement in HCV pathogenesis and HCC were unknown, and our analysis suggests novel contributions of Core and PA28γ to the functions of these proteins.

Our observations were then used to prioritize potential candidates for the follow-up experimental investigations. Cellular assays based on siRNA knockdowns of selected candidates in the HCV infected and replicon cells validated VTI1A, a SNARE protein associated with vesicular transport, which was upregulated in CoreTG but not in PA28$\gamma^{-/-}$CoreTG, as a novel regulator of HCV propagation but not replication. VTIA-deficient mice are largely indistinguishable from the normal mice except for minor growth retardation in a few instances; therefore, VTI1A is a promising novel candidate for anti-HCV therapy.

Our analysis not only builds on the present understanding of the Core-PA28γ interplay in HCV infection but also provides novel insights that would facilitate the clinical evaluation of proteomic changes associated with HCV pathogenesis. Our analysis also provides a generic framework for investigating large scale proteomic data. Such investigation may help identify common themes associated with different physiological conditions, especially pathogen (such as viral) infection and disease, and help develop effective broad spectrum strategies aimed at ameliorating pathogen infection and diseases.

ASSOCIATED CONTENT

Supporting Information

This material is available free of charge via the Internet at http://pubs.acs.org.

AUTHOR INFORMATION

Corresponding Author

*Tel: +81-72-641-9890. Fax: +81-72-641-9881. E-mail: kenji@nibio.go.jp.

Author Contributions

‖These authors contributed equally to this work.

Notes

The authors declare no competing financial interest.

ACKNOWLEDGMENTS

This study was supported by the Industrial Technology Research Grant Program in 2007 from New Energy and Industrial Technology Development Organization (NEDO) of Japan and also by grants-in-aid from the Ministry of Health, Labor, and Welfare; the Ministry of Education, Culture, Sports, Science, and Technology; the Osaka University Global Center of Excellence Program; and the Foundation for Biomedical Research and Innovation. We gratefully acknowledge Dr. T. Wakita for providing us with cell lines and plasmids.

REFERENCES

(1) Dubuisson, J. Hepatitis C virus proteins. *World J. Gastroenterol.* **2007**, *13* (17), 2406–15.

(2) Moriishi, K.; Mochizuki, R.; Moriya, K.; Miyamoto, H.; Mori, Y.; Abe, T.; Murata, S.; Tanaka, K.; Miyamura, T.; Suzuki, T.; Koike, K.; Matsuura, Y. Critical role of PA28gamma in hepatitis C virus-associated steatogenesis and hepatocarcinogenesis. *Proc. Natl. Acad. Sci. U.S.A.* **2007**, *104* (5), 1661–6.

(3) Myrmel, H.; Ulvestad, E.; Asjo, B. The hepatitis C virus enigma. *APMIS* **2009**, *117* (5–6), 427–39.

(4) Tang, H.; Grise, H. Cellular and molecular biology of HCV infection and hepatitis. *Clin. Sci. (London)* **2009**, *117* (2), 49–65.

(5) Moradpour, D.; Penin, F.; Rice, C. M. Replication of hepatitis C virus. *Nat. Rev. Microbiol.* **2007**, *5* (6), 453–63.

(6) Simmonds, P.; Bukh, J.; Combet, C.; Deleage, G.; Enomoto, N.; Feinstone, S.; Halfon, P.; Inchauspe, G.; Kuiken, C.; Maertens, G.; Mizokami, M.; Murphy, D. G.; Okamoto, H.; Pawlotsky, J. M.; Penin, F.; Sablon, E.; Shin, I. T.; Stuyver, L. J.; Thiel, H. J.; Viazov, S.; Weiner, A. J.; Widell, A. Consensus proposals for a unified system of nomenclature of hepatitis C virus genotypes. *Hepatology* **2005**, *42* (4), 962–73.

(7) De Francesco, R.; Migliaccio, G. Challenges and successes in developing new therapies for hepatitis C. *Nature* **2005**, *436* (7053), 953–60.
(8) Kato, N.; Mori, K.; Abe, K.; Dansako, H.; Kuroki, M.; Ariumi, Y.; Wakita, T.; Ikeda, M. Efficient replication systems for hepatitis C virus using a new human hepatoma cell line. *Virus Res.* **2009**, *146* (1–2), 41–50.
(9) Murray, C. L.; Rice, C. M. Hepatitis C: An unsuspected drug target. *Nature* **2010**, *465* (7294), 42–4.
(10) Mori, Y.; Moriishi, K.; Matsuura, Y. Hepatitis C virus core protein: its coordinate roles with PA28gamma in metabolic abnormality and carcinogenicity in the liver. *Int. J. Biochem. Cell Biol.* **2008**, *40* (8), 1437–42.
(11) Gao, G.; Luo, H. The ubiquitin-proteasome pathway in viral infections. *Can. J. Physiol. Pharmacol.* **2006**, *84* (1), 5–14.
(12) Miyamoto, H.; Moriishi, K.; Moriya, K.; Murata, S.; Tanaka, K.; Suzuki, T.; Miyamura, T.; Koike, K.; Matsuura, Y. Involvement of the PA28gamma-dependent pathway in insulin resistance induced by hepatitis C virus core protein. *J. Virol.* **2007**, *81* (4), 1727–35.
(13) Moriishi, K.; Okabayashi, T.; Nakai, K.; Moriya, K.; Koike, K.; Murata, S.; Chiba, T.; Tanaka, K.; Suzuki, R.; Suzuki, T.; Miyamura, T.; Matsuura, Y. Proteasome activator PA28gamma-dependent nuclear retention and degradation of hepatitis C virus core protein. *J. Virol.* **2003**, *77* (19), 10237–49.
(14) Moriishi, K.; Shoji, I.; Mori, Y.; Suzuki, R.; Suzuki, T.; Kataoka, C.; Matsuura, Y. Involvement of PA28gamma in the propagation of hepatitis C virus. *Hepatology* **2010**, *52* (2), 411–20.
(15) Suzuki, R.; Moriishi, K.; Fukuda, K.; Shirakura, M.; Ishii, K.; Shoji, I.; Wakita, T.; Miyamura, T.; Matsuura, Y.; Suzuki, T. Proteasomal turnover of hepatitis C virus core protein is regulated by two distinct mechanisms: a ubiquitin-dependent mechanism and a ubiquitin-independent but PA28gamma-dependent mechanism. *J. Virol.* **2009**, *83* (5), 2389–92.
(16) Chen, Y. A.; Tripathi, L. P.; Mizuguchi, K. TargetMine, an integrated data warehouse for candidate gene prioritisation and target discovery. *PLoS One* **2011**, *6* (3), e17844.
(17) Liu, M. C.; Akle, V.; Zheng, W.; Dave, J. R.; Tortella, F. C.; Hayes, R. L.; Wang, K. K. Comparing calpain- and caspase-3-mediated degradation patterns in traumatic brain injury by differential proteome analysis. *Biochem. J.* **2006**, *394* (Pt 3), 715–25.
(18) Stark, C.; Breitkreutz, B. J.; Reguly, T.; Boucher, L.; Breitkreutz, A.; Tyers, M. BioGRID: a general repository for interaction datasets. *Nucleic Acids Res.* **2006**, *34* (Database issue), D535–9.
(19) Turner, B.; Razick, S.; Turinsky, A. L.; Vlasblom, J.; Crowdy, E. K.; Cho, E.; Morrison, K.; Donaldson, I. M.; Wodak, S. J. iRefWeb: interactive analysis of consolidated protein interaction data and their supporting evidence. *Database (Oxford)* **2010**, *2010*, baq023.
(20) Cline, M. S.; Smoot, M.; Cerami, E.; Kuchinsky, A.; Landys, N.; Workman, C.; Christmas, R.; Avila-Campilo, I.; Creech, M.; Gross, B.; Hanspers, K.; Isserlin, R.; Kelley, R.; Killcoyne, S.; Lotia, S.; Maere, S.; Morris, J.; Ono, K.; Pavlovic, V.; Pico, A. R.; Vailaya, A.; Wang, P. L.; Adler, A.; Conklin, B. R.; Hood, L.; Kuiper, M.; Sander, C.; Schmulevich, I.; Schwikowski, B.; Warner, G. J.; Ideker, T.; Bader, G. D. Integration of biological networks and gene expression data using Cytoscape. *Nat. Protoc.* **2007**, *2* (10), 2366–82.
(21) Assenov, Y.; Ramirez, F.; Schelhorn, S. E.; Lengauer, T.; Albrecht, M. Computing topological parameters of biological networks. *Bioinformatics* **2008**, *24* (2), 282–4.
(22) Tripathi, L. P.; Kataoka, C.; Taguwa, S.; Moriishi, K.; Mori, Y.; Matsuura, Y.; Mizuguchi, K. Network based analysis of hepatitis C virus Core and NS4B protein interactions. *Mol. Biosyst.* **2010**, *6* (12), 2539–53.
(23) Ashburner, M.; Ball, C. A.; Blake, J. A.; Botstein, D.; Butler, H.; Cherry, J. M.; Davis, A. P.; Dolinski, K.; Dwight, S. S.; Eppig, J. T.; Harris, M. A.; Hill, D. P.; Issel-Tarver, L.; Kasarskis, A.; Lewis, S.; Matese, J. C.; Richardson, J. E.; Ringwald, M.; Rubin, G. M.; Sherlock, G. Gene ontology: tool for the unification of biology. The Gene Ontology Consortium. *Nat. Genet.* **2000**, *25* (1), 25–9.
(24) Aoki-Kinoshita, K. F.; Kanehisa, M. Gene annotation and pathway mapping in KEGG. *Methods Mol. Biol.* **2007**, *396*, 71–91.
(25) McKusick-Nathans Institute of Genetic Medicine, Johns Hopkins Medicine (Baltimore, MD) and National Center for Biotechnology Information, National Library of Medicine (Bethesda, MD), Online Mendelian Inheritance in Man, OMIM (TM). In 2010.
(26) Benjamini, Y.; Hochberg, Y. Controlling the false discovery rate-A practical and powerful approach to multiple testing. *J. R. Statist. Soc. B* **1995**, *57* (1), 289–300.
(27) Noble, W. S. How does multiple testing correction work? *Nat. Biotechnol.* **2009**, *27* (12), 1135–7.
(28) Linhart, C.; Halperin, Y.; Shamir, R. Transcription factor and microRNA motif discovery: the Amadeus platform and a compendium of metazoan target sets. *Genome Res.* **2008**, *18* (7), 1180–9.
(29) Montgomery, S. B.; Griffith, O. L.; Sleumer, M. C.; Bergman, C. M.; Bilenky, M.; Pleasance, E. D.; Prychyna, Y.; Zhang, X.; Jones, S. J. ORegAnno: an open access database and curation system for literature-derived promoters, transcription factor binding sites and regulatory variation. *Bioinformatics* **2006**, *22* (5), 637–40.
(30) Okamoto, T.; Omori, H.; Kaname, Y.; Abe, T.; Nishimura, Y.; Suzuki, T.; Miyamura, T.; Yoshimori, T.; Moriishi, K.; Matsuura, Y. A single-amino-acid mutation in hepatitis C virus NS5A disrupting FKBP8 interaction impairs viral replication. *J. Virol.* **2008**, *82* (7), 3480–9.
(31) Pietschmann, T.; Lohmann, V.; Kaul, A.; Krieger, N.; Rinck, G.; Rutter, G.; Strand, D.; Bartenschlager, R. Persistent and transient replication of full-length hepatitis C virus genomes in cell culture. *J. Virol.* **2002**, *76* (8), 4008–21.
(32) Kato, T.; Date, T.; Miyamoto, M.; Furusaka, A.; Tokushige, K.; Mizokami, M.; Wakita, T. Efficient replication of the genotype 2a hepatitis C virus subgenomic replicon. *Gastroenterology* **2003**, *125* (6), 1808–17.
(33) Wakita, T.; Pietschmann, T.; Kato, T.; Date, T.; Miyamoto, M.; Zhao, Z.; Murthy, K.; Habermann, A.; Krausslich, H. G.; Mizokami, M.; Bartenschlager, R.; Liang, T. J. Production of infectious hepatitis C virus in tissue culture from a cloned viral genome. *Nat. Med.* **2005**, *11* (7), 791–6.
(34) Cao, W.; Sun, B.; Feitelson, M. A.; Wu, T.; Tur-Kaspa, R.; Fan, Q. Hepatitis C virus targets over-expression of arginase I in hepatocarcinogenesis. *Int. J. Cancer* **2009**, *124* (12), 2886–92.
(35) Tacke, R. S.; Tosello-Trampont, A.; Nguyen, V.; Mullins, D. W.; Hahn, Y. S. Extracellular hepatitis C virus core protein activates STAT3 in human monocyte/macrophage/dendritic cells via an IL-6 autocrine pathway. *J. Biol. Chem.* **2011**, DOI: 10.1074/jbc.M110.217653 .
(36) Waris, G.; Turkson, J.; Hassanein, T.; Siddiqui, A. Hepatitis C virus (HCV) constitutively activates STAT-3 via oxidative stress: role of STAT-3 in HCV replication. *J. Virol.* **2005**, *79* (3), 1569–80.
(37) Randall, G.; Panis, M.; Cooper, J. D.; Tellinghuisen, T. L.; Sukhodolets, K. E.; Pfeffer, S.; Landthaler, M.; Landgraf, P.; Kan, S.; Lindenbach, B. D.; Chien, M.; Weir, D. B.; Russo, J. J.; Ju, J.; Brownstein, M. J.; Sheridan, R.; Sander, C.; Zavolan, M.; Tuschl, T.; Rice, C. M. Cellular cofactors affecting hepatitis C virus infection and replication. *Proc. Natl. Acad. Sci. U.S.A.* **2007**, *104* (31), 12884–9.
(38) Lin, W.; Kim, S. S.; Yeung, E.; Kamegaya, Y.; Blackard, J. T.; Kim, K. A.; Holtzman, M. J.; Chung, R. T. Hepatitis C virus core protein blocks interferon signaling by interaction with the STAT1 SH2 domain. *J. Virol.* **2006**, *80* (18), 9226–35.
(39) Tsutsumi, T.; Suzuki, T.; Moriya, K.; Shintani, Y.; Fujie, H.; Miyoshi, H.; Matsuura, Y.; Koike, K.; Miyamura, T. Hepatitis C virus core protein activates ERK and p38 MAPK in cooperation with ethanol in transgenic mice. *Hepatology* **2003**, *38* (4), 820–8.
(40) Nanda, S. K.; Herion, D.; Liang, T. J. The SH3 binding motif of HCV [corrected] NS5A protein interacts with Bin1 and is important for apoptosis and infectivity. *Gastroenterology* **2006**, *130* (3), 794–809.
(41) Jacobs, J. M.; Diamond, D. L.; Chan, E. Y.; Gritsenko, M. A.; Qian, W.; Stastna, M.; Baas, T.; Camp, D. G., 2nd; Carithers, R. L., Jr.; Smith, R. D.; Katze, M. G. Proteome analysis of liver cells expressing a full-length hepatitis C virus (HCV) replicon and biopsy specimens of

posttransplantation liver from HCV-infected patients. *J. Virol.* **2005**, *79* (12), 7558–69.
(42) Woodhouse, S. D.; Narayan, R.; Latham, S.; Lee, S.; Antrobus, R.; Gangadharan, B.; Luo, S.; Schroth, G. P.; Klenerman, P.; Zitzmann, N. Transcriptome sequencing, microarray, and proteomic analyses reveal cellular and metabolic impact of hepatitis C virus infection in vitro. *Hepatology* **2010**, *52* (2), 443–53.
(43) Fujino, T.; Nakamuta, M.; Yada, R.; Aoyagi, Y.; Yasutake, K.; Kohjima, M.; Fukuizumi, K.; Yoshimoto, T.; Harada, N.; Yada, M.; Kato, M.; Kotoh, K.; Taketomi, A.; Maehara, Y.; Nakashima, M.; Enjoji, M. Expression profile of lipid metabolism-associated genes in hepatitis C virus-infected human liver. *Hepatol. Res.* **2010**, *40* (9), 923–9.
(44) MacPherson, J. I.; Sidders, B.; Wieland, S.; Zhong, J.; Targett-Adams, P.; Lohmann, V.; Backes, P.; Delpuech-Adams, O.; Chisari, F.; Lewis, M.; Parkinson, T.; Robertson, D. L. An integrated transcriptomic and meta-analysis of hepatoma cells reveals factors that influence susceptibility to HCV infection. *PLoS One* **2011**, *6* (10), e25584.
(45) de Chassey, B.; Navratil, V.; Tafforeau, L.; Hiet, M. S.; Aublin-Gex, A.; Agaugue, S.; Meiffren, G.; Pradezynski, F.; Faria, B. F.; Chantier, T.; Le Breton, M.; Pellet, J.; Davoust, N.; Mangeot, P. E.; Chaboud, A.; Penin, F.; Jacob, Y.; Vidalain, P. O.; Vidal, M.; Andre, P.; Rabourdin-Combe, C.; Lotteau, V. Hepatitis C virus infection protein network. *Mol. Syst. Biol.* **2008**, *4*, 230.
(46) Chazal, N.; Gerlier, D. Virus entry, assembly, budding, and membrane rafts. *Microbiol. Mol. Biol. Rev.* **2003**, *67* (2), 226–37.
(47) Manes, S.; del Real, G.; Martinez, A. C. Pathogens: raft hijackers. *Nat. Rev. Immunol.* **2003**, *3* (7), 557–68.
(48) Riethmuller, J.; Riehle, A.; Grassme, H.; Gulbins, E. Membrane rafts in host-pathogen interactions. *Biochim. Biophys. Acta* **2006**, *1758* (12), 2139–47.
(49) Suzuki, T.; Suzuki, Y. Virus infection and lipid rafts. *Biol. Pharm. Bull.* **2006**, *29* (8), 1538–41.
(50) Mannova, P.; Fang, R.; Wang, H.; Deng, B.; McIntosh, M. W.; Hanash, S. M.; Beretta, L. Modification of host lipid raft proteome upon hepatitis C virus replication. *Mol. Cell. Proteomics* **2006**, *5* (12), 2319–25.
(51) Corless, L.; Crump, C. M.; Griffin, S. D.; Harris, M. Vps4 and the ESCRT-III complex are required for the release of infectious hepatitis C virus particles. *J. Gen. Virol.* **2010**, *91* (Pt 2), 362–72.
(52) Lai, C. K.; Jeng, K. S.; Machida, K.; Lai, M. M. Hepatitis C virus egress and release depend on endosomal trafficking of core protein. *J. Virol.* **2010**, *84* (21), 11590–8.
(53) Jahn, R.; Scheller, R. H. SNAREs—engines for membrane fusion. *Nat. Rev. Mol. Cell. Biol.* **2006**, *7* (9), 631–43.
(54) Kreykenbohm, V.; Wenzel, D.; Antonin, W.; Atlachkine, V.; von Mollard, G. F. The SNAREs vti1a and vti1b have distinct localization and SNARE complex partners. *Eur. J. Cell Biol.* **2002**, *81* (5), 273–80.
(55) Kunwar, A. J.; Rickmann, M.; Backofen, B.; Browski, S. M.; Rosenbusch, J.; Schoning, S.; Fleischmann, T.; Krieglstein, K.; Fischer von Mollard, G. Lack of the endosomal SNAREs vti1a and vti1b led to significant impairments in neuronal development. *Proc. Natl. Acad. Sci. U.S.A.* **2011**, *108* (6), 2575–80.
(56) Mascia, L.; Langosch, D. Evidence that late-endosomal SNARE multimerization complex is promoted by transmembrane segments. *Biochim. Biophys. Acta* **2007**, *1768* (3), 457–66.
(57) Offenhauser, C.; Lei, N.; Roy, S.; Collins, B. M.; Stow, J. L.; Murray, R. Z. Syntaxin 11 binds Vti1b and regulates late endosome to lysosome fusion in macrophages. *Traffic* **2011**, *12*, 762–73.
(58) Bryceson, Y. T.; Chiang, S. C.; Darmanin, S.; Fauriat, C.; Schlums, H.; Theorell, J.; Wood, S. M. Molecular mechanisms of natural killer cell activation. *J. Innate Immun.* **2011**, *3* (3), 216–26.
(59) Arneson, L. N.; Brickshawana, A.; Segovis, C. M.; Schoon, R. A.; Dick, C. J.; Leibson, P. J. Cutting edge: syntaxin 11 regulates lymphocyte-mediated secretion and cytotoxicity. *J. Immunol.* **2007**, *179* (6), 3397–401.
(60) Dabrazhynetskaya, A.; Ma, J.; Guerreiro-Cacais, A. O.; Arany, Z.; Rudd, E.; Henter, J. I.; Karre, K.; Levitskaya, J.; Levitsky, V. Syntaxin 11 marks a distinct intracellular compartment recruited to the immunological synapse of NK cells to co-localize with cytotoxic granules. *J. Cell. Mol. Med.* **2011**, *16*, 129–41.
(61) Gholam, C.; Grigoriadou, S.; Gilmour, K. C.; Gaspar, H. B. Familial haemophagocytic lymphohistiocytosis: advances in the genetic basis, diagnosis and management. *Clin. Exp. Immunol.* **2011**, *163* (3), 271–83.
(62) How, P. C.; Shields, D. Tethering function of the caspase cleavage fragment of Golgi protein p115 promotes apoptosis via a p53-dependent pathway. *J. Biol. Chem.* **2011**, *286* (10), 8565–76.
(63) Radulescu, A. E.; Mukherjee, S.; Shields, D. The Golgi protein p115 associates with gamma-tubulin and plays a role in Golgi structure and mitosis progression. *J. Biol. Chem.* **2011**, *286* (24), 21915–26.
(64) Bouffard, P.; Hayashi, P. H.; Acevedo, R.; Levy, N.; Zeldis, J. B. Hepatitis C virus is detected in a monocyte/macrophage subpopulation of peripheral blood mononuclear cells of infected patients. *J. Infect. Dis.* **1992**, *166* (6), 1276–80.
(65) Roxrud, I.; Raiborg, C.; Pedersen, N. M.; Stang, E.; Stenmark, H. An endosomally localized isoform of Eps15 interacts with Hrs to mediate degradation of epidermal growth factor receptor. *J. Cell Biol.* **2008**, *180* (6), 1205–18.
(66) Salcini, A. E.; Chen, H.; Iannolo, G.; De Camilli, P.; Di Fiore, P. P. Epidermal growth factor pathway substrate 15, Eps15. *Int. J. Biochem. Cell Biol.* **1999**, *31* (8), 805–9.
(67) Barnaba, V. Hepatitis C virus infection: a "liaison a trois" amongst the virus, the host, and chronic low-level inflammation for human survival. *J. Hepatol.* **2010**, *53* (4), 752–61.
(68) Hiroishi, K.; Ito, T.; Imawari, M. Immune responses in hepatitis C virus infection and mechanisms of hepatitis C virus persistence. *J. Gastroenterol. Hepatol.* **2008**, *23* (10), 1473–82.
(69) Kawai, T.; Akira, S. Toll-like receptor and RIG-I-like receptor signaling. *Ann. N.Y. Acad. Sci.* **2008**, *1143*, 1–20.
(70) Sklan, E. H.; Charuworn, P.; Pang, P. S.; Glenn, J. S. Mechanisms of HCV survival in the host. *Nat. Rev. Gastroenterol. Hepatol.* **2009**, *6* (4), 217–27.
(71) Szabo, G.; Dolganiuc, A. Hepatitis C and innate immunity: recent advances. *Clin. Liver Dis.* **2008**, *12* (3), 675–92.
(72) Taylor, D. R.; Silberstein, E. Innate immunity and hepatitis C virus: eluding the host cell defense. *Front. Biosci.* **2009**, *14*, 4950–61.
(73) Legarda-Addison, D.; Hase, H.; O'Donnell, M. A.; Ting, A. T. NEMO/IKKgamma regulates an early NF-kappaB-independent cell-death checkpoint during TNF signaling. *Cell Death Differ.* **2009**, *16* (9), 1279–88.
(74) Ye, X.; Lu, H.; Huo, K.; Chen, D. Finding a novel interacting protein of the hepatic carcinoma related gene MIP: NF-kappaB essential modulator (NEMO). *Oncol. Rep.* **2011**, *25* (1), 231–5.
(75) Beraza, N.; Malato, Y.; Sander, L. E.; Al-Masaoudi, M.; Freimuth, J.; Riethmacher, D.; Gores, G. J.; Roskams, T.; Liedtke, C.; Trautwein, C. Hepatocyte-specific NEMO deletion promotes NK/NKT cell- and TRAIL-dependent liver damage. *J. Exp. Med.* **2009**, *206* (8), 1727–37.
(76) Cruz-Munoz, M. E.; Veillette, A. Do NK cells always need a license to kill? *Nat. Immunol.* **2010**, *11* (4), 279–80.
(77) Wang, K.; Song, Y.; Chen, D. B.; Zheng, J. Protein phosphatase 3 differentially modulates vascular endothelial growth factor- and fibroblast growth factor 2-stimulated cell proliferation and signaling in ovine fetoplacental artery endothelial cells. *Biol. Reprod.* **2008**, *79* (4), 704–10.
(78) Singh, A. P.; Bafna, S.; Chaudhary, K.; Venkatraman, G.; Smith, L.; Eudy, J. D.; Johansson, S. L.; Lin, M. F.; Batra, S. K. Genome-wide expression profiling reveals transcriptomic variation and perturbed gene networks in androgen-dependent and androgen-independent prostate cancer cells. *Cancer Lett.* **2008**, *259* (1), 28–38.
(79) Ostenfeld, M. S.; Bramsen, J. B.; Lamy, P.; Villadsen, S. B.; Fristrup, N.; Sorensen, K. D.; Ulhoi, B.; Borre, M.; Kjems, J.; Dyrskjot, L.; Orntoft, T. F. miR-145 induces caspase-dependent and -independent cell death in urothelial cancer cell lines with targeting of an expression signature present in Ta bladder tumors. *Oncogene* **2010**, *29* (7), 1073–84.

(80) Johansen, C.; Vestergaard, C.; Kragballe, K.; Kollias, G.; Gaestel, M.; Iversen, L. MK2 regulates the early stages of skin tumor promotion. *Carcinogenesis* **2009**, *30* (12), 2100–8.
(81) Wang, C.; Zhou, J.; Wang, S.; Ye, M.; Fan, G.; Zou, H.; Jiang, C. Shotgun approach based comparative proteomic analysis of levo-tetrahydropalmatine-induced apoptosis in hepatocytes. *Toxicol. Lett.* **2010**, *194* (1–2), 8–15.
(82) Del Campo, J. A.; Romero-Gomez, M. Steatosis and insulin resistance in hepatitis C: a way out for the virus? *World J. Gastroenterol.* **2009**, *15* (40), 5014–9.
(83) Douglas, M. W.; George, J. Molecular mechanisms of insulin resistance in chronic hepatitis C. *World J. Gastroenterol.* **2009**, *15* (35), 4356–64.
(84) Shintani, Y.; Fujie, H.; Miyoshi, H.; Tsutsumi, T.; Tsukamoto, K.; Kimura, S.; Moriya, K.; Koike, K. Hepatitis C virus infection and diabetes: direct involvement of the virus in the development of insulin resistance. *Gastroenterology* **2004**, *126* (3), 840–8.
(85) Cao, X.; Pobezinskaya, Y. L.; Morgan, M. J.; Liu, Z. G. The role of TRADD in TRAIL-induced apoptosis and signaling. *FASEB J.* **2011**, *25* (4), 1353–8.
(86) Zheng, L.; Bidere, N.; Staudt, D.; Cubre, A.; Orenstein, J.; Chan, F. K.; Lenardo, M. Competitive control of independent programs of tumor necrosis factor receptor-induced cell death by TRADD and RIP1. *Mol. Cell. Biol.* **2006**, *26* (9), 3505–13.
(87) Tellinghuisen, T. L.; Foss, K. L.; Treadaway, J. Regulation of hepatitis C virion production via phosphorylation of the NSSA protein. *PLoS Pathog.* **2008**, *4* (3), e1000032.
(88) Benedicto, I.; Molina-Jimenez, F.; Bartosch, B.; Cosset, F. L.; Lavillette, D.; Prieto, J.; Moreno-Otero, R.; Valenzuela-Fernandez, A.; Aldabe, R.; Lopez-Cabrera, M.; Majano, P. L. The tight junction-associated protein occludin is required for a postbinding step in hepatitis C virus entry and infection. *J. Virol.* **2009**, *83* (16), 8012–20.
(89) Bantel, H.; Schulze-Osthoff, K. Apoptosis in hepatitis C virus infection. *Cell Death Differ.* **2003**, *10* (Suppl 1), S48–58.
(90) Deng, L.; Adachi, T.; Kitayama, K.; Bungyoku, Y.; Kitazawa, S.; Ishido, S.; Shoji, I.; Hotta, H. Hepatitis C virus infection induces apoptosis through a Bax-triggered, mitochondrion-mediated, caspase 3-dependent pathway. *J. Virol.* **2008**, *82* (21), 10375–85.
(91) Fischer, R.; Baumert, T.; Blum, H. E. Hepatitis C virus infection and apoptosis. *World J. Gastroenterol.* **2007**, *13* (36), 4865–72.
(92) Hanafy, S. M.; Shehata, O. H.; Farahat, N. M. Expression of apoptotic markers BCL-2 and Bax in chronic hepatitis C virus patients. *Clin. Biochem.* **2010**, *43* (13–14), 1112–7.
(93) Joyce, M. A.; Walters, K. A.; Lamb, S. E.; Yeh, M. M.; Zhu, L. F.; Kneteman, N.; Doyle, J. S.; Katze, M. G.; Tyrrell, D. L. HCV induces oxidative and ER stress, and sensitizes infected cells to apoptosis in SCID/Alb-uPA mice. *PLoS Pathog.* **2009**, *5* (2), e1000291.
(94) Kondo, Y.; Machida, K.; Liu, H. M.; Ueno, Y.; Kobayashi, K.; Wakita, T.; Shimosegawa, T.; Lai, M. M. Hepatitis C virus infection of T cells inhibits proliferation and enhances fas-mediated apoptosis by down-regulating the expression of CD44 splicing variant 6. *J. Infect. Dis.* **2009**, *199* (5), 726–36.
(95) Anupam, R.; Datta, A.; Kesic, M.; Green-Church, K.; Shkriabai, N.; Kvaratskhelia, M.; Lairmore, M. D. Human T-lymphotropic virus type 1 p30 interacts with REGgamma and modulates ATM (ataxia telangiectasia mutated) to promote cell survival. *J. Biol. Chem.* **2011**, *286* (9), 7661–8.
(96) Mao, I.; Liu, J.; Li, X.; Luo, H. REGgamma, a proteasome activator and beyond? *Cell. Mol. Life Sci.* **2008**, *65* (24), 3971–80.
(97) Tian, M.; Xiaoyi, W.; Xiaotao, L.; Guosheng, R. Proteasomes reactivator REG gamma enchances oncogenicity of MDA-MB-231 cell line via promoting cell proliferation and inhibiting apoptosis. *Cell. Mol. Biol. (Noisy-le-Grand)* **2009**, *55* (Suppl), OL1121–31.
(98) Zannini, L.; Buscemi, G.; Fontanella, E.; Lisanti, S.; Delia, D. REGgamma/PA28gamma proteasome activator interacts with PML and Chk2 and affects PML nuclear bodies number. *Cell Cycle* **2009**, *8* (15), 2399–407.
(99) Samuelsen, J. T.; Schwarze, P. E.; Huitfeldt, H. S.; Thrane, E. V.; Lag, M.; Refsnes, M.; Skarpen, E.; Becher, R. Regulation of rat alveolar type 2 cell proliferation in vitro involves type II cAMP-dependent protein kinase. *Am. J. Physiol. Lung Cell. Mol. Physiol.* **2007**, *292* (1), L232–9.
(100) Bungyoku, Y.; Shoji, I.; Makine, T.; Adachi, T.; Hayashida, K.; Nagano-Fujii, M.; Ide, Y. H.; Deng, L.; Hotta, H. Efficient production of infectious hepatitis C virus with adaptive mutations in cultured hepatoma cells. *J. Gen. Virol.* **2009**, *90* (Pt 7), 1681–91.
(101) Lemon, S. M.; McKeating, J. A.; Pietschmann, T.; Frick, D. N.; Glenn, J. S.; Tellinghuisen, T. L.; Symons, J.; Furman, P. A. Development of novel therapies for hepatitis C. *Antiviral Res.* **2010**, *86* (1), 79–92.
(102) Lin, K. Development of novel antiviral therapies for hepatitis C virus. *Virol. Sin.* **2010**, *25* (4), 246–66.
(103) Chan, S. C.; Lo, S. Y.; Liou, J. W.; Lin, M. C.; Syu, C. L.; Lai, M. J.; Chen, Y. C.; Li, H. C. Visualization of the structures of the hepatitis C virus replication complex. *Biochem. Biophys. Res. Commun.* **2011**, *404* (1), 574–8.
(104) Dreyer, J. L. Lentiviral vector-mediated gene transfer and RNA silencing technology in neuronal dysfunctions. *Mol. Biotechnol.* **2011**, *47* (2), 169–87.
(105) Camm, E. J.; Martin-Gronert, M. S.; Wright, N. L.; Hansell, J. A.; Ozanne, S. E.; Giussani, D. A. Prenatal hypoxia independent of undernutrition promotes molecular markers of insulin resistance in adult offspring. *FASEB J.* **2011**, *25* (1), 420–7.
(106) Ning, B. F.; Ding, J.; Yin, C.; Zhong, W.; Wu, K.; Zeng, X.; Yang, W.; Chen, Y. X.; Zhang, J. P.; Zhang, X.; Wang, H. Y.; Xie, W. F. Hepatocyte nuclear factor 4 alpha suppresses the development of hepatocellular carcinoma. *Cancer Res.* **2010**, *70* (19), 7640–51.
(107) Niehof, M.; Borlak, J. EPS15R, TASP1, and PRPF3 are novel disease candidate genes targeted by HNF4alpha splice variants in hepatocellular carcinomas. *Gastroenterology* **2008**, *134* (4), 1191–202.
(108) Hussain, K. M.; Leong, K. L.; Ng, M. M.; Chu, J. J. The essential role of clathrin-mediated endocytosis in the infectious entry of human enterovirus 71. *J. Biol. Chem.* **2011**, *286* (1), 309–21.
(109) Helle, F.; Dubuisson, J. Hepatitis C virus entry into host cells. *Cell. Mol. Life Sci.* **2008**, *65* (1), 100–12.
(110) Marshall, A.; Rushbrook, S.; Morris, L. S.; Scott, I. S.; Vowler, S. L.; Davies, S. E.; Coleman, N.; Alexander, G. Hepatocyte expression of minichromosome maintenance protein-2 predicts fibrosis progression after transplantation for chronic hepatitis C virus: a pilot study. *Liver Transpl.* **2005**, *11* (4), 427–33.
(111) Bard-Chapeau, E. A.; Li, S.; Ding, J.; Zhang, S. S.; Zhu, H. H.; Princen, F.; Fang, D. D.; Han, T.; Bailly-Maitre, B.; Poli, V.; Varki, N. M.; Wang, H.; Feng, G. S. Ptpn11/Shp2 acts as a tumor suppressor in hepatocellular carcinogenesis. *Cancer Cell* **2011**, *19* (5), 629–39.
(112) Matsuo, K.; Delibegovic, M.; Matsuo, I.; Nagata, N.; Liu, S.; Bettaieb, A.; Xi, Y.; Araki, K.; Yang, W.; Kahn, B. B.; Neel, B. G.; Haj, F. G. Altered glucose homeostasis in mice with liver-specific deletion of Src homology phosphatase 2. *J. Biol. Chem.* **2010**, *285* (51), 39750–8.
(113) Rios, E. J.; Piliponsky, A. M.; Ra, C.; Kalesnikoff, J.; Galli, S. J. Rabaptin-5 regulates receptor expression and functional activation in mast cells. *Blood* **2008**, *112* (10), 4148–57.
(114) Stenmark, H.; Vitale, G.; Ullrich, O.; Zerial, M. Rabaptin-5 is a direct effector of the small GTPase Rab5 in endocytic membrane fusion. *Cell* **1995**, *83* (3), 423–32.
(115) Edamoto, Y.; Hara, A.; Biernat, W.; Terracciano, L.; Cathomas, G.; Riehle, H. M.; Matsuda, M.; Fujii, H.; Scoazec, J. Y.; Ohgaki, H. Alterations of RB1, p53 and Wnt pathways in hepatocellular carcinomas associated with hepatitis C, hepatitis B and alcoholic liver cirrhosis. *Int. J. Cancer* **2003**, *106* (3), 334–41.
(116) Laurent-Puig, P.; Zucman-Rossi, J. Genetics of hepatocellular tumors. *Oncogene* **2006**, *25* (27), 3778–86.
(117) Park, K. J.; Choi, S. H.; Koh, M. S.; Kim, D. J.; Yie, S. W.; Lee, S. Y.; Hwang, S. B. Hepatitis C virus core protein potentiates c-Jun N-terminal kinase activation through a signaling complex involving TRADD and TRAF2. *Virus Res.* **2001**, *74* (1–2), 89–98.
(118) Kawaguchi, T.; Yoshida, T.; Harada, M.; Hisamoto, T.; Nagao, Y.; Ide, T.; Taniguchi, E.; Kumemura, H.; Hanada, S.; Maeyama, M.;

Baba, S.; Koga, H.; Kumashiro, R.; Ueno, T.; Ogata, H.; Yoshimura, A.; Sata, M. Hepatitis C virus down-regulates insulin receptor substrates 1 and 2 through up-regulation of suppressor of cytokine signaling 3. *Am. J. Pathol.* **2004**, *165* (5), 1499–508.

(119) Ma, Z.; Liu, Z.; Wu, R. F.; Terada, L. S. p66(Shc) restrains Ras hyperactivation and suppresses metastatic behavior. *Oncogene* **2010**, *29* (41), 5559–67.

(120) Spoden, G. A.; Rostek, U.; Lechner, S.; Mitterberger, M.; Mazurek, S.; Zwerschke, W. Pyruvate kinase isoenzyme M2 is a glycolytic sensor differentially regulating cell proliferation, cell size and apoptotic cell death dependent on glucose supply. *Exp. Cell Res.* **2009**, *315* (16), 2765–74.

OPEN ACCESS Freely available online

PLOS ONE

Protein Kinase C Regulates Human Pluripotent Stem Cell Self-Renewal

Masaki Kinehara[1], Suguru Kawamura[1], Daiki Tateyama[1], Mika Suga[1], Hiroko Matsumura[1], Sumiyo Mimura[1], Noriko Hirayama[2], Mitsuhi Hirata[1], Kozue Uchio-Yamada[3], Arihiro Kohara[2], Kana Yanagihara[1], Miho K. Furue[1]*

1 Laboratory of Stem Cell Cultures, Department of Disease Bioresources Research, National Institute of Biomedical Innovation, Ibaraki, Osaka, Japan, **2** Laboratory of Cell Cultures, Department of Disease Bioresources Research, National Institute of Biomedical Innovation, Ibaraki, Osaka, Japan, **3** Laboratory of Animal Models for Human Diseases, Department of Disease Bioresources Research, National Institute of Biomedical Innovation, Ibaraki, Osaka, Japan

Abstract

Background: The self-renewal of human pluripotent stem (hPS) cells including embryonic stem and induced pluripotent stem cells have been reported to be supported by various signal pathways. Among them, fibroblast growth factor-2 (FGF-2) appears indispensable to maintain self-renewal of hPS cells. However, downstream signaling of FGF-2 has not yet been clearly understood in hPS cells.

Methodology/Principal Findings: In this study, we screened a kinase inhibitor library using a high-throughput alkaline phosphatase (ALP) activity-based assay in a minimal growth factor-defined medium to understand FGF-2-related molecular mechanisms regulating self-renewal of hPS cells. We found that in the presence of FGF-2, an inhibitor of protein kinase C (PKC), GF109203X (GFX), increased ALP activity. GFX inhibited FGF-2-induced phosphorylation of glycogen synthase kinase-3β (GSK-3β), suggesting that FGF-2 induced PKC and then PKC inhibited the activity of GSK-3β. Addition of activin A increased phosphorylation of GSK-3β and extracellular signal-regulated kinase-1/2 (ERK-1/2) synergistically with FGF-2 whereas activin A alone did not. GFX negated differentiation of hPS cells induced by the PKC activator, phorbol 12-myristate 13-acetate whereas Gö6976, a selective inhibitor of PKCα, β, and γ isoforms could not counteract the effect of PMA. Intriguingly, functional gene analysis by RNA interference revealed that the phosphorylation of GSK-3β was reduced by siRNA of PKCδ, PKCε, and ζ, the phosphorylation of ERK-1/2 was reduced by siRNA of PKCε and ζ, and the phosphorylation of AKT was reduced by PKCε in hPS cells.

Conclusions/Significance: Our study suggested complicated cross-talk in hPS cells that FGF-2 induced the phosphorylation of phosphatidylinositol-3 kinase (PI3K)/AKT, mitogen-activated protein kinase/ERK-1/2 kinase (MEK), PKC/ERK-1/2 kinase, and PKC/GSK-3β. Addition of GFX with a MEK inhibitor, U0126, in the presence of FGF-2 and activin A provided a long-term stable undifferentiated state of hPS cells even though hPS cells were dissociated into single cells for passage. This study untangles the cross-talk between molecular mechanisms regulating self-renewal and differentiation of hPS cells.

Citation: Kinehara M, Kawamura S, Tateyama D, Suga M, Matsumura H, et al. (2013) Protein Kinase C Regulates Human Pluripotent Stem Cell Self-Renewal. PLoS ONE 8(1): e54122. doi:10.1371/journal.pone.0054122

Editor: Tadayuki Akagi, Kanazawa University, Japan

Received April 20, 2012; **Accepted** December 10, 2012; **Published** January 21, 2013

Funding: The funders had no role in study design, data collection and analysis, decision to publish, or preparation of the manuscript. This study was supported by grants-in-aid from the Ministry of Health, Labor and Welfare of Japan to M.K.F. and A.K., the Ministry of Education, Culture, Sports, Science and Technology of Japan to M.K.F. and M.K. and the Japan Science and Technology Agency to M.K.F.

Competing Interests: The authors have read the journal's policy and have the following conflicts: One of the authors, (MKF) has declared a financial interest in a company, Cell Science & Technology Institute Corporation (Sendai, Japan) whose product, a basal medium ESF was used in this study. However, the licensing fee is less than $10,000 per year. This does not alter the authors adherence to all the PLOS ONE policies on sharing data and materials.

* E-mail: mkfurue@nibio.go.jp

Introduction

The self-renewal of human pluripotent stem (hPS) cells including embryonic stem (hES) and induced pluripotent stem (hiPS) cells have been reported to be supported by various signal pathways, including transforming growth factor-β/activin A/Nodal [1–3], sphingosine-1-phosphate/platelet derived growth factor (S1P/PDGF) [4], insulin growth factor (IGF)/insulin [5] and fibroblast growth factor-2 (FGF-2) [6–9]. The process of self-renewal appears to be regulated synergistically through the various pathways via growth factor or cytokine supplementation. Among them, FGF-2 signaling appears indispensable to hPS cells [10–12].

FGF family members including FGF-2, bind to FGF receptors (FGFRs) and induce activation of the mitogen-activated protein kinase/extracellular signal-regulated kinase-1/2 (ERK-1/2) kinase (MEK), phosphatidylinositol-3 kinase (PI3K), and phospholipase C-γ (PLC-γ)/protein kinase C (PKC) pathways [13]. MEK-1/2 activation by FGFR results in ERK-1/2 phosphorylation, which subsequently translocates into the nucleus leading to phosphorylation of transcription factors such as c-Myc, c-Jun, and c-Fos. PI3K, a lipid kinase activates pleckstrin homology (PH) domain containing proteins such as AKT, and 3-phosphoinositide-dependent kinase-1 (PDK1). AKT directly activates murine double minute 2 (MDM2), a negative regulator of p53. p53 is

responsible for DNA damage surveillance and in response initiates cell cycle arrest and DNA repair. Interestingly, AKT also inhibits glycogen synthase kinase-3 (GSK-3), a negative regulator of Wnt signaling by phosphorylation [14]. However, the contributions of FGF-2 downstream pathways in the self-renewal of hPS cells have been controversial [9,14–18]. The ERK pathway has been thought to promote cell proliferation and adhesion but also differentiation in hES cells. The PI3K pathway plays important roles in proliferation, differentiation, survival, and cellular transformation.

Previously, we found that a proteoglycan, heparin promotes FGF-2 activity on the growth of undifferentiated hES cells in a minimal growth factor-defined culture medium, hESF9 [8], in which the effect of exogenous factors can be analyzed without the confounding influences of undefined components [8,19–23] because insulin, transferrin, albumin conjugated with oleic acid, and FGF-2 (10 ng/ml) are the only protein components. Understanding cell signaling in undifferentiated hPS cells has lead to the development of optimal conditions for culturing hPS cells. However, manipulation of hPS cells still remains difficult because hPS cells as a single cell are unstable of self-renewal. Although Rho-associated kinase (ROCK) inhibitor (Y-27632) is quite effective to markedly diminish dissociation-induced apoptosis of single cells of hPS cells [24], the continuous use of the ROCK inhibitor increases differentiated cells [25]. For developing application using hPS cells, such as cell based therapy or toxicity screening tests, handling cell numbers would be beneficial. Even for basic research, handling cell numbers would be useful when the cells are dissociated for passages or differentiation. Presumably, if the culture conditions were able to fully support undifferentiated state, even single cells might maintain undifferentiated state. We suspected that there were unrevealed mechanisms to maintain undifferentiated state of single hPS cells. To further understand FGF-2 related molecular mechanisms regulating self-renewal would enhance understanding unclarified cell signaling in hPS cells. Therefore, we screened a kinase inhibitor library using a high-throughput alkaline phosphatase (ALP) activity-based assay in a minimal growth factor-defined culture medium, hESF9. We found that in the presence of FGF-2, an inhibitor of PKCs, GF109203X (GFX), increased ALP activity, suggesting that PKC reduces self-renewal of hPS cells. GFX inhibited FGF-2-induced GSK-3β phosphorylation. Addition of activin A increased phosphorylation of GSK-3β and ERK-1/2 synergistically with FGF-2 whereas activin A alone did not induce phosphorylation of GSK-3β. GFX negated differentiation of hPS cells induced by a PKC activator, phorbol 12-myristate 13-acetate (PMA) whereas Gö6976, a selective inhibitor of PKCα, β, and γ isoforms did not counteract the effect of PMA. Functional gene analysis by RNA interference revealed that siRNA of PKCδ, ε, and ζ isoforms decreased phosphorylation of GSK-3β and also siRNA of PKCε and ζ isoforms decreased phosphorylation of ERK-1/2 in hPS cells. siRNA of PKCε decreased phosphorylation of AKT. On the basis of these results, we suggest that PKCδ, ε and ζ isoforms are FGF-2 downstream effectors, and they play various roles in regulating hPS cell self-renewal. This study helps to untangle the cross-talk between molecular mechanisms regulating self-renewal and differentiation of hPS cells.

Results

PKC inhibitor increased ALP activity of hiPS cells

Previously, we detected the cell proliferative effect of heparin on hES cells without feeder cells in a minimal growth factor-defined culture medium, hESF9 [8], in which the effect of exogenous factors can be analyzed without the confounding influences of undefined components [8,19–23]. In this culture condition using hESF9 medium (Table S1) on bovine fibronectin (FN), a high-throughput ALP activity-based assay was performed to evaluate a library of chemical kinase inhibitors to understand FGF-2 related molecular mechanisms regulating self-renewal of hPS cells. Nine compounds were found to increase ALP activity of the hiPS cell line 201B7 [26] (Fig. 1): Kenpaullone, which is a substitute for a reprogramming factor KLF-4 in mouse iPS cells [27]; Y-27632, which is a Rho-kinase (ROCK) inhibitor known to enhance hES cells survival [24]; HA-1004, H-89, and HA-1077, which are kinase inhibitors presumed to target ROCK [28]; GF109203X (GFX) [29], which is a inhibitor for PKC isoforms; and H-7, H-8, and H-9, which are also thought to target PKC [30]. These results suggest that FGF-2 induces PKC, and PKC acts downstream of FGF-2 to regulate self-renewal of hPS cells.

Effect of PKC inhibitor on FGF-2 signaling in hPS cells

To examine how GFX influenced FGF-2 signaling in hPS cells, the phosphorylation of AKT, ERK-1/2, and GSK-3β induced by FGF-2 with GFX was confirmed by western blotting analysis (Fig. S1A, S1B, S1C, S1D). Then, the phosphorylation levels were quantified by AlphaScreen® SureFire® assay kit. Human ES cells H9 [31] after starvation of FGF-2 and insulin were treated with FGF-2 with and without GFX. FGF-2 significantly stimulated the phosphorylation of AKT, ERK-1/2, and GSK-3β in H9 cells in 15 minutes (Fig. 2A, 2B, 2C) as described previously [16,32]. Addition of GFX at 5.0 μM in the presence of FGF-2 significantly increased AKT phosphorylation in 15 minutes compared with addition of FGF-2 alone (Fig. 2A, 2B, Fig. S1E). The level of ERK-1/2 phosphorylation induced by FGF-2 with GFX was comparable with that without GFX (Fig. 2A). On the other hand, FGF-2-induced GSK-3β phosphorylation was completely inhibited by GFX (Fig. 2A, 2B) at concentrations higher than 1 μM treatment (Fig. S1E).

Addition of the PI3K inhibitor LY-294002 with FGF-2 completely inhibited AKT phosphorylation and significantly reduced GSK-3β phosphorylation (Fig. 2B, Fig. S1B). Addition of the MEK inhibitor U0126 with FGF-2 reduced ERK-1/2 phosphorylation and had little influence on GSK-3β phosphorylation. Addition of the GSK inhibitor BIO with FGF-2 signifi-

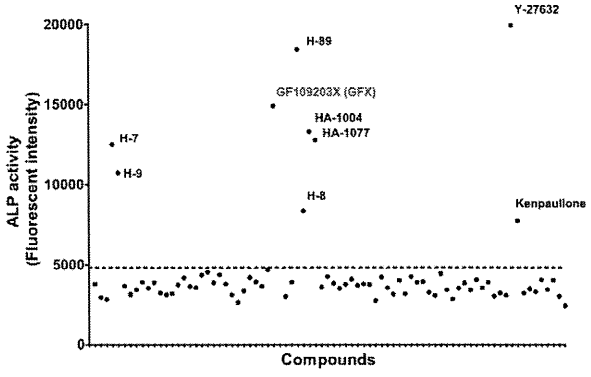

Figure 1. An ALP activity-based high-throughput screening assay of chemical library for PKC inhibitors. The ALP activity using 4-methylumbelliferyl phosphate [59] in 201B7 hiPS cells in a 96-well plate was measured by fluorometry. Each dot on the graph represents the fluorescent intensity for each compound of the kinase inhibitor library. Dotted line indicates the level for DMSO as a control.
doi:10.1371/journal.pone.0054122.g001

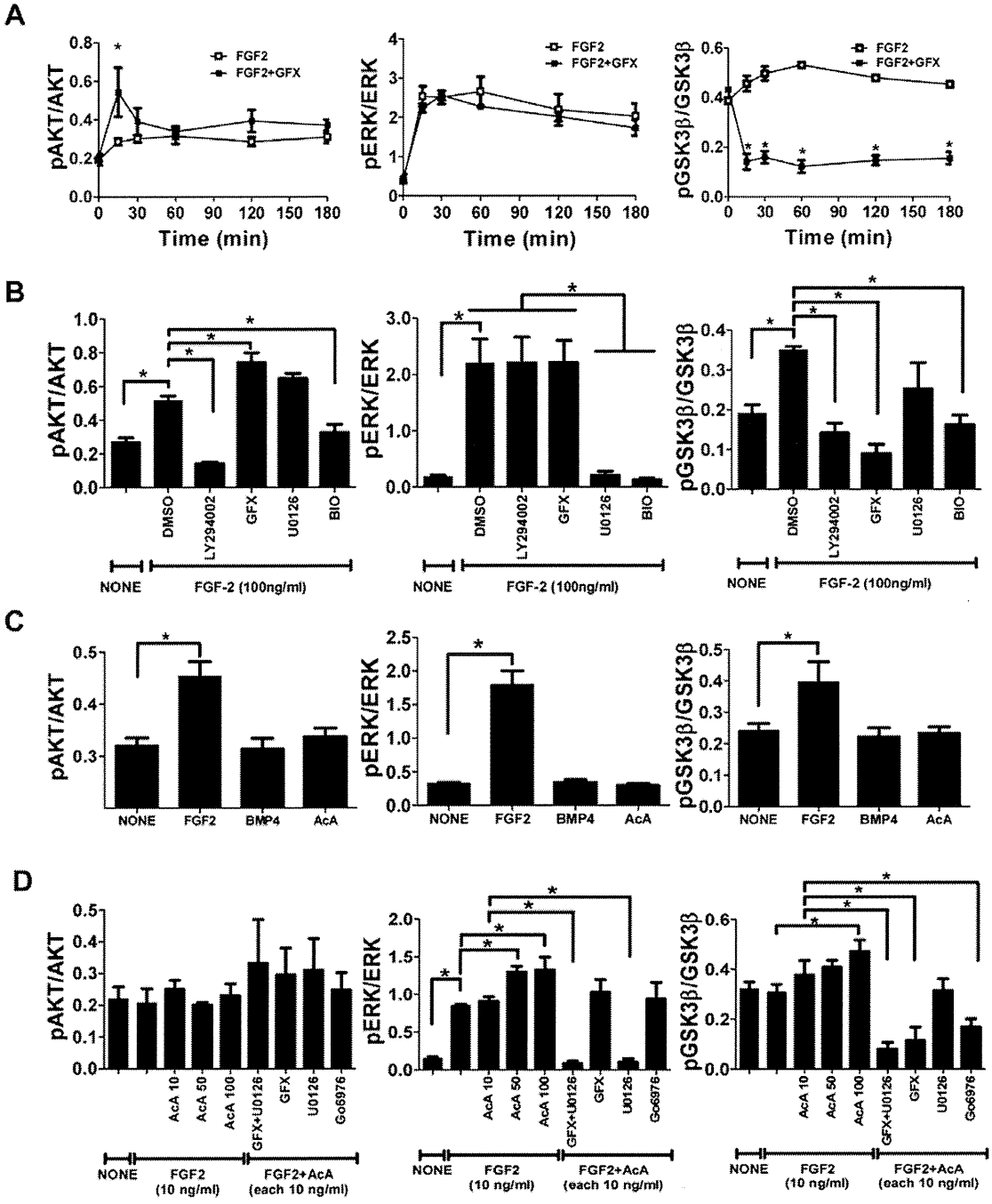

Figure 2. Effect of PKC inhibitor on FGF-2 signaling in hPS cells. The phosphorylation levels in H9 hES cells were measured by AlphaScreen® SureFire® assay kit. The values of the y-axis are the ratio of each phosphorylation to each total signal protein. (A) The cells were stimulated with FGF-2 (100 ng/ml) in fresh medium without insulin after overnight starvation and incubated with (open square) or without GFX (5 μM, closed square) for 180 minutes. The data are represented as means ± SE (n = 3). *P<0.05. (B) The cells were stimulated with FGF-2 (100 ng/ml) in fresh medium without insulin after overnight starvation. Fifteen minutes after FGF-2 addition together with each inhibitor as indicated on the panel. The data are represented as means ± SE (n = 3). *P<0.05. (C) The cells were treated with FGF-2 (100 ng/ml), BMP-4 (100 ng/ml) or activin A (100 ng/ml) in fresh medium without insulin after overnight starvation. Fifteen minutes after the addition of each growth factor as indicated on the panel. The data are represented as means ± SE (n = 3). *P<0.05. (D) The cells after growth factor starvation were stimulated with FGF-2 (10 ng/ml) and activin A (10 or 100 ng/ml) together with U0126 (5 μM) and GFX (5 μM) or Gö6976 (5 μM) in fresh medium without insulin for 15 minutes. Fifteen minutes after the addition of each growth factor/inhibitor as indicated on the panel. The data are represented as means ± SE (n = 3). *P<0.05.
doi:10.1371/journal.pone.0054122.g002

cantly reduced phosphorylation of not only AKT, but also ERK-1/2 and GSK-3β.

Neither BMP-4 nor activin A in the absence of FGF-2 induced the phosphorylation of AKT, ERK-1/2, or GSK-3β in 201B7 iPS cells (Fig. 2C, Fig. S1C). From our previous report that activin A acts synergistically with FGF-2 in stimulating the phosphorylation of ERK-1/2 [20], we speculated that activin A may increase the phosphorylation of GSK-3β synergistically with FGF-2. Addition

of increasing concentrations of activin A with FGF-2 increased phosphorylation of both GSK-3β and ERK-1/2 in a dose-dependent manner in H9 hES cells (Fig. 2D, Fig. S1D). Addition of U0126 with FGF-2 and activin A had little influence on phosphorylation of both AKT and GSK-3β, and completely inhibited phosphorylation of ERK-1/2. Addition of GFX together with U0126 in the presence of FGF-2 and activin A not significantly increased phosphorylation of AKT, while it completely inhibited phosphorylation of both ERK-1/2 and GSK-3β (Fig. 2D, Fig. S1D). A selective inhibitor of classical PKC (α, β, and γ isoforms) [29], Gö6976 had little influence on phosphorylation of AKT and decreased phosphorylation of GSK-3β less than GFX. These results suggested that FGF-2-induced PKC stimulated phosphorylation of GSK-3β and that GFX inhibited the PKC-induced phosphorylation of GSK-3β, but it increased phosphorylation of AKT (Fig. S2).

Effect of GFX and PMA on colony morphology of the cells

To confirm the speculation that PKCs play roles in regulating self-renewal in hPS cells, the effect of the PKC activator PMA with several kinase inhibitors on the culture of 201B7 hiPS cells was determined (Fig. 3A). Treatment with PMA scattered the iPS cell colony dramatically. PMA-treatment with LY-294002, lithium chloride (LiCl, GSK inhibitor), Y-27632, or U0126 did not reverse the morphological change whereas GFX negated the effect of PMA on cultured 201B7 cells. Gö6976 did not negate the effect of PKC. The effect of Gö6976 was compared with that of GFX on ALP-activity of the cells: GFX with FGF-2 increased the ALP-activity of 201B7 iPS cells, while Gö6976 with FGF-2 had little effect on ALP-activity of the cells (Fig. 3B). GFX increased colony forming efficiency in hESF9 medium (Fig. 3C). Gö6976 did not increase the colony sizes of 201B7 cells and also cell numbers of H9 and 201B7 cells whereas GFX increased the colony sizes and also cell numbers (Fig. 3D, 3E, 3F). PMA activates PKCα, β, γ, δ, ε, η, and θ whereas GFX inhibits PKCα, β, γ, δ, ε, and ζ isoforms. Gö6976 inhibits PKCα, β, and γ isoforms. These results and findings suggested that PKCδ or ε isoforms regulate undifferentiated state of hPS cells.

Isoform-specific function of PKCs in FGF-2 signaling

To determine the isoform-specific function of PKCs on FGF-2 signaling, at first the expression of 11 PKC isoform genes in 201B7 iPS cells was determined by RT-PCR. The results showed that the cells expressed all of 11 PKC isoforms examined here (Fig. 4A). The PKC inhibitor results described above suggested that PKCδ or PKCε might be responsible for GSK-3β phosphorylation but there is a possibility that PKCζ might also be involved. Then, we examined whether FGF-2 stimulated phosphorylation of PKCδ, PKCε or PKCζ with or without GFX. Image analysis of western blotting showed that the phosphorylation of PKCδ and PKCε was increased in a time-dependent manner after stimulation of FGF-2 and the phosphorylation of PKCζ was increased in 15 min after stimulation of FGF-2 and then decreased, suggesting that activation mechanism of PKCζ might be related with GSK-3β phosphorylation (Fig. 4B). GFX diminished the increased phosphorylation of all three PKCs. These result indicated that FGF-2 induced PKCδ, PKCε, and PKCζ in hPS cells.

We next examined the effects of short interfering RNA (siRNA) targeting PKCδ, PKCε or PKCζ on FGF-2 signaling in 201B7 iPS cells. The efficacy and specificity of siRNA was confirmed by quantitative RT-PCR (Fig. S3A). The expression of the targeted PKC genes was inhibited for at least 60%. The phosphorylation levels of AKT, ERK-1/2 and GSK-3β were measured in these PKCs-knockdown cells by AlphaScreen® SureFire® assay kit. The results showed that knockdown of PKCδ, and PKCζ did not affect FGF-2-induced AKT phosphorylation while knockdown of PKCε significantly reduced it (Fig. 4C). Knockdown of either PKCε or PKCζ isoform significantly decreased FGF-2-induced ERK-1/2 phosphorylation. GFX which is reported to target PKCα, β, γ, δ, ε and ζ isoforms did not change the level of FGF-2-induced ERK-1/2 phosphorylation, as shown above (Fig. 2 and Fig. S1). These results implied that cross-interaction among PKC isoforms might affect on the level of FGF-2-induced ERK-1/2 phosphorylation. Then, the cells were treated with the inhibitory peptide cocktail for all isoforms (PKCα, β, γ, δ, ε and ζ), or the inhibitory peptide cocktail for PKCδ, ε, and ζ. The inhibitory peptide cocktail for all isoforms did not affect on FGF-2-induced ERK-1/2 phosphorylation. On the other hand, the inhibitory peptide cocktail for PKCδ, ε, and ζ inhibited the ERK-1/2 phosphorylation (Fig. S4). These results suggested that inhibitions of all isoforms neutralized the reducing effect on FGF-2-induced ERK-1/2 phosphorylation by the inhibition of PKCε and ζ. GSK-3β phosphorylation was significantly reduced by the knockdown of all three PKC isoforms, compared with that by non-target siRNA. These results suggest that FGF-2 induced PKCs, followed by phosphorylation of ERK-1/2 and GSK-3β in hPS cells (Fig. S3B). From these results, we showed that FGF-2 induced PKCδ, ε, and ζ, resulting in stimulation of differentiation in hPS cells which might cause instability of the self-renewal state of hPS cells and that GFX targets these PKC isoforms in hPS cells, resulting in enhanced self-renewal of hPS cells.

Stability of self-renewal of hPS cells in the presence of inhibitors of ERK-1/2 and PKC

Based on the results above, we hypothesized that inhibition of both PKC and ERK-1/2 might provide stable culture of hPS cells in our minimal defined medium hESF9 with activin A. Dissociated single hPS cells were inoculated on FN in hESF9 medium supplemented with activin A (10 ng/ml) [8,20], U0126 (5 μM) or GFX (5 μM). When dissociated single cells were cultured in hESF9, hESF9 + activin A, hESF9 + U0126, or hESF9 + activin A + U0126, many cells died or differentiated (Fig. 5A). On the other hand, when dissociated single cells were cultured in hESF9 + activin A + GFX, or hESF9 + activin A + GFX + U0126 (2i), cells could proliferate enough to be passaged. However, usually after 3 passages, epithelial-like cells appeared in the culture of hESF9 + activin A + GFX condition (Fig. S5A). Immunocytochemical analysis by image analyzer showed that ratio of OCT3/4-positive cell population in the culture of hESF9 + activin A + GFX + U0126 (2i) condition was slightly higher than that in the culture of hESF9 + activin A + GFX (Fig. S5B and S5C). Gene expression in the cells cultured in these culture conditions was analyzed by real-time PCR (Fig. 5B). The expression of an endoderm marker, FOXA2, and a mesoderm marker, T were increased by activin A but it was significantly reduced by the addition of U0126. When the cells were cultured in hESF9 + activin A + U0126 + GFX, both FOXA2 and T were inhibited at lower level and also the undifferentiated makers, NANOG and OCT3/4 were maintained at higher ratio in the cells than those in other culture conditions. Next, the serial culture of dissociated single cells of hES H9, hES KhES4, hiPS 201B7 and hiPS Tic [33] cell lines were tested in hESF9 medium supplemented with activin A (10 ng/ml), U0126 (5 μM) and GFX (5 μM) (designated hESF9a_{2i} medium; Table S1). Dissociated single hPS cells were grown on FN in hESF9a_{2i} medium for 3 passages. Phase-contrast image showed that cell morphology seemed undifferentiated although they did not form hPS typical cell colony. OCT3/4 expression profiles were confirmed by immunofluorescence analysis using image analyzer,

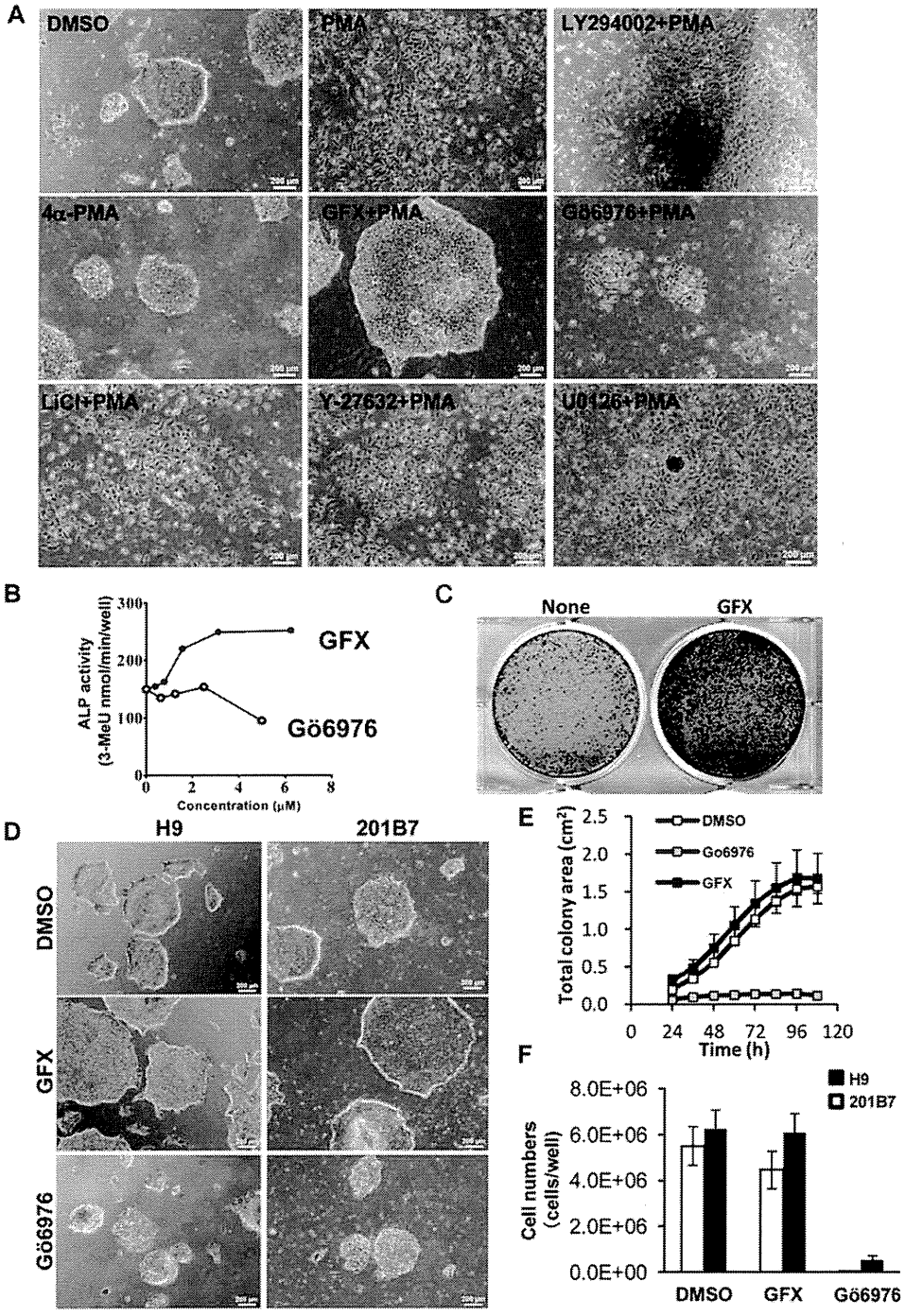

Figure 3. The effect of PKC on the morphologies of hPS cells with or without GFX. (A) Phase-contrast image of 201B7 hiPS cells cultured in feeder-free hESF9 defined medium on FN 24 hours after treatment with DMSO, PMA (10 nM), 4α-PMA (10 nM), GFX (5 μM), PMA (10 nM) with GFX (5 μM), PMA (10 nM) with Gö6976 (5 μM), PMA (10 nM) with LY-294002 (50 μM), PMA (10 nM) with LiCl (1 mM), PMA (10 nM) with Y-27632 (10 μM), or PMA (10 nM) with U0126 (20 μM). An inactive PMA analogue, 4α-PMA is used as negative control. Scale bars, 200 μm. (B) Quantitative ALP-based assay of 201B7 hiPS cells cultured in feeder-free hESF9 medium with GFX (closed circle) or Gö6976 (open circle) as indicated concentrations. (C) Colony forming efficiency of dissociated single hPS cells cultured with or without GFX. Dissociated single 201B7 cells seeded at 250,000 cells/well were grown on a 6-well plate coated with FN (2 μg/cm^2) in hESF9 medium supplemented with and without 1 μM GFX. A in 5 days and stained with ALP fast-red substrate. (D) Phase-contrast image of 201B7 hiPS cells or H9 hES cells cultured in feeder-free hESF9 medium with DMSO (open square), GFX (5 μM, gray square), or Gö6976 (5 μM, closed square). (E) Growth of cell colony area of hPS cells in the presence of GFX or Gö6976. The whole images of 201B7 cell colonies grown in a 6-well-plate coated with FN in the presence of DMSO, GFX or Gö6976 in hESF9 medium was measured by an analysis software, Cell-Quant. The images were captured every 12 hours in live cell imaging system Biostation CT. The data are represented as means ± SD (n = 3). (**F**) Cell growth of hPS cells in the presence of GFX or Gö6976. The numbers of H9 (open bars) and 201B7 cells (closed bars) grown in a 6-well-plate coated with FN in the presence of DMSO, GFX or Gö6976 in hESF9 medium were counted on 5 days. The data are represented as means ± SD (n = 3).

doi:10.1371/journal.pone.0054122.g003

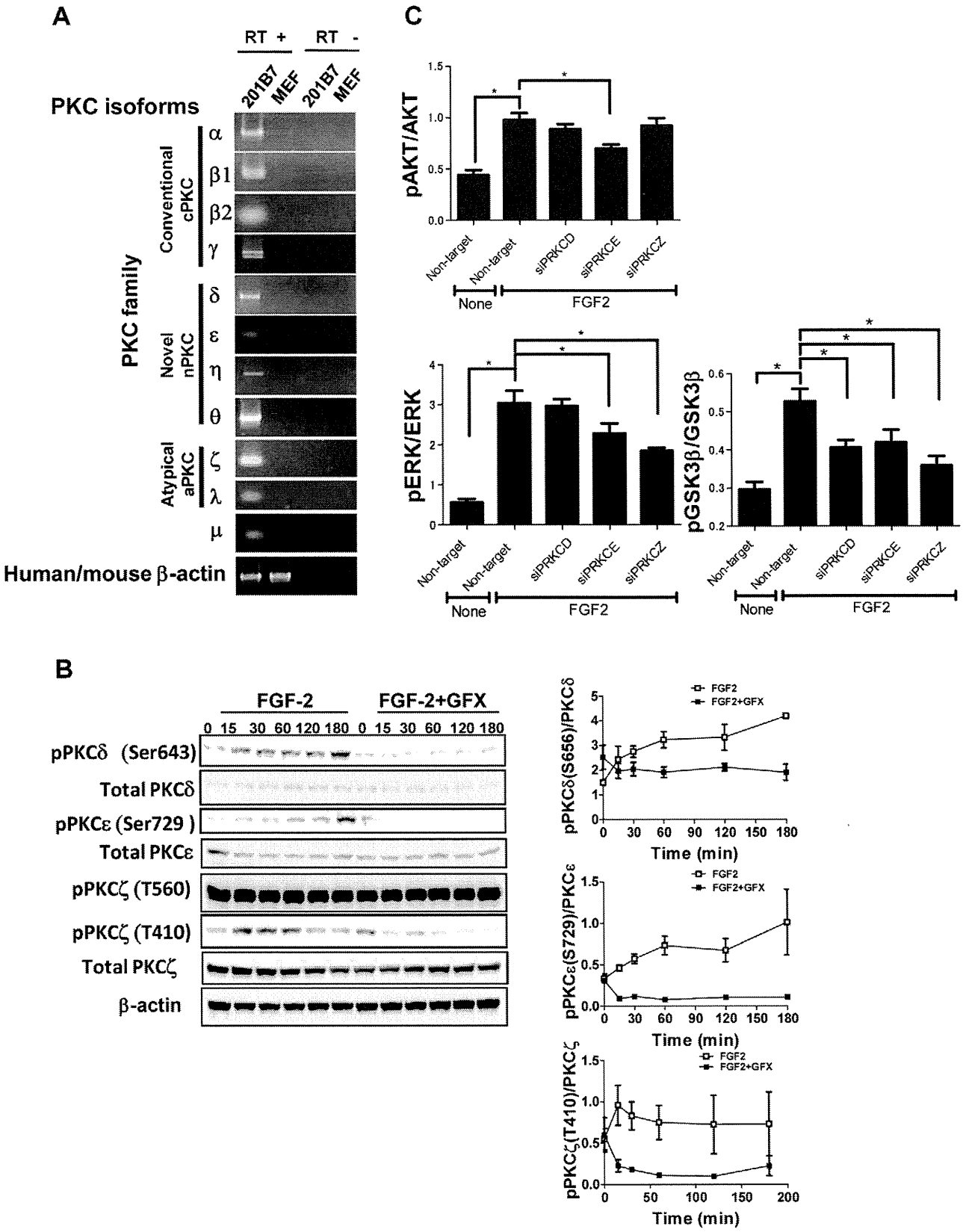

Figure 4. Specific-isoform of PKCs function in FGF-2 signaling. (**A**) RT-PCR analysis of PKC isoform expression. Total RNA was extracted from the undifferentiated 201B7 hiPS cells cultured on feeder cells (CF-1) with KSR-based medium or the feeder cells. Primers were listed in Table S3. (**B**) Phosphorylation of PKCδ, ε, or ζ isoforms induced by FGF-2 (open square) with GFX (closed square). 201B7 hiPS cells were stimulated with FGF-2 (100 ng/ml) after overnight starvation and incubated with or without GFX (5 μM) for 180 minutes. The cells were lysed and followed by western blot

analysis using an antibody detecting the phosphorylation or total protein amount of PKCδ, PKCε, or PKCζ. Protein content quantified from the gel blot images (n = 3). The values of the y-axis are the ratio of each phosphorylation to each total signal protein. (**C**) FGF-2 signaling in hPS cells with specific PKC isoforms-targeting siRNA. 201B7 iPS cells were transfected with specific PKCδ, ε, or ζ isoforms-targeting siRNA or non-targeting siRNA. The phosphorylation levels of the cells treated with FGF-2(100 ng/ml) after overnight starvation were measured by AlphaScreen® SureFire® assay kit. The values of the y-axis are the ratio of each phosphorylation to each total signal protein. The data are represented as means ± SE (n = 3). *P<0.05.
doi:10.1371/journal.pone.0054122.g004

suggesting that the hPS cells maintained undifferentiated state. Another undifferentiated maker, TRA-1-60 expression was also confirmed in hPS cells grown in hESF9a$_{2i}$ medium for 3 passages (Fig. S6).

Serial culture more than 10 passages of undifferentiated H9 hES cells and 201B7 hiPS were tested on FN in hESF9a$_{2i}$ medium. Undifferentiated morphologies of 201B7 hiPS (Fig. S7A) and H9 hES colonies (Fig. S8A) were maintained for more than 30 passages using the conventional passage procedure. The growth rates of H9 hES and 201B7 hiPS cells in hESF9a$_{2i}$ medium were similar to those of cells grown in the conventional KSR-based medium on feeders (Figs. S7B and S8B). The cells retained expression of stage-specific embryonic antigen (SSEA)-4 [34], cell surface antigens TRA-1-60 [35], TRA-1-81 [35], CD90 (Thy-1) [36], and TRA-2-54 [36] (alkaline phosphatase), but did not express SSEA-1 [37] or a neural marker A2B5 [36] (Fig. S7C, S7D and S8C, S8D). The cells retained normal karyotypes (Fig. S9A), pluripotency in vitro (Fig. S9B) and in vivo (Fig. S9C). These results confirmed that inhibition of both ERK-1/2 and PKC supported the self-renewal of hPS cells.

Discussion

Many studies reported that FGF-2 activates both the MAPK/ERK, and PI3K/AKT pathways, which are important for maintaining pluripotency and viability in hPS cells [9,14–16]. However, FGF-2 downstream signaling is not clearly understood in hPS cells. In this study using a minimum essential defined culture system [8,20], we showed that FGF-2 activated PI3K/AKT and MEK/ERK-1/2, but also PKCδ, ε and ζ isoforms in hPS cells (Fig. 6).

The PKC family has been implicated as an intracellular mediator of several neurotransmitters, hormones, tumor promoters, α1-adrenergic agonists, and phorbol esters, and it is important in the regulation of growth, differentiation, cell death, and neurotransmission [38]. The PKC family comprises classical (PKCα, β, and γ; activated by Ca^{2+} and phorbol esters), novel PKC (PKCδ, ε, η, and θ; activated by phorbol esters but not regulated by Ca^{2+}), and atypical PKC (PKCζ and PKCι/λ; not activated by Ca^{2+} or phorbol esters). Different isoforms may perform distinct functions, as suggested by their differential pattern of localization, differences in condition of activation, and some differences in substrate specificity [39–40]. PKC has previously been implicated in GSK-3 regulation [41–42]. Fang et al. [43] showed that PKCα, βII, γ, η, and δ were capable of phosphorylating GSK-3β while PKCε and PKCζ did not phosphorylate GSK-3 by in vitro kinase assays; also, expression of constitutively active PKCα, βI, γ, η enhanced phosphorylation of cotransfected GSK-3β in HEK293 cells. On the other hand, Eng et al. [15] reported that negative construct of PKCε isoform prevented phosphorylation of GSK-3 in migrating fibroblasts. These pieces of evidence suggested that specific isoforms of PKC have different roles in different types of cells. Shuibing et al. [44] reported that activation of PKCα and/or β directs the pancreatic specification of hES cells. Recently, Feng et al. [45] reported that activation of PKCδ induces extraembryonic endoderm differentiation of hES cells. These studies suggested that PKCs might be involved in differentiation of hPS cells. Our study showed that FGF-2 induced PKCδ, ε, and ζ, resulting in phosphorylation of GSK-3β, ERK-1/2, or AKT. Chou, et al. [46] reported that the phosphorylation of PKCζ was regulated by PI3-kinase and PDK-1 in NIH 3T3 fibroblasts. Intriguingly, PKCζ can stimulate GSK-3 activity, by relieving PKB-imposed inhibition [47]. In mouse ES cells, it has been shown that PKCζ plays an important role in inducing lineage commitment in mESCs through a PKCζ–nuclear factor kappa-light-chain-enhancer of activated B cells signaling axis [48]. However, PKC inhibition does not change phosphorylation of ERK-1/2 or GSK-3β. In view of the fact that LIF mainly regulates self-renewal in mouse ES cells, isoform specific function might be cross-regulated by other signaling in the cells. Further, our study showed that the combination effect by inhibition of PKCα, β, γ, δ, ε, and ζ was different from that by inhibition of PKCε and ζ, suggesting that each PKC might interact in different contexts and also PKCδ, ε, and ζ might have different activation mechanisms in hPS cells. It is needed further investigation in future.

GSK-3β is inhibited by phosphorylation stimulated by the canonical Wnt signal pathway, which is followed by the accumulation of β-catenin to the nucleus [49]. From the above findings, it follows that FGF-2 may activate Wnt signaling through PKC leading to differentiation of hPS cells. This conclusion contradicts the findings of previous studies demonstrating that canonical Wnt signaling supports self-renewal of stem cells [50–52]. However, it is consistent with a study showing that canonical Wnt signaling does not appear to promote stem cell maintenance, which prevents differentiation of stem cells [53]. On the other hand, some studies have shown a dual function for Wnt signaling in hES cells in that the pathways of self-renewal or differentiation are dependent on the presence of hES cell supporting factors [51–52]. Recently, Ding et al. [32] showed that FGF-2 modulates Wnt signaling through AKT/GSK-3β signaling and suggested that the differences in the results could be due to the culture platform. Our findings suggest that GSK-3β activity is regulated by FGF-2 through both PI3K/AKT and PKC pathways. AKT/GSK-3β signaling may support self-renewal whereas PKC/GSK-3β may promote cell differentiation of hPS cells. However, GFX decreased the phosphorylation level of GSK-3β to lower level than non-treatment. GSK-3β signaling might be stimulated also by other signal pathway in hPS cells. Target genes of these pathways and further regulation mechanisms in GSK-3β signaling should be analyzed in future.

TGF-β/activin/nodal pathways are thought to crosstalk with FGF signaling in regulating hPS cells. Vallier et al. [1–2,54] demonstrated that activin/nodal pathway in co-operation with FGF-2 is necessary for the maintenance of pluripotency in hES cells. We recently reported that activin A enhances FGF-2-induced ERK-1/2, which permits neural and mesendodermal differentiation of hES cells [20]. In this study we showed that activin A enhanced FGF-2-induced phosphorylation of not only ERK-1/2 but also GSK-3β. Inhibition of these pathways provided stable culture of hPS cells for long-term. In this study, we used both GFX and U0126 to inhibit these pathways. GFX targeting all of PKCα, β, γ, δ, ε, and ζ had no inhibitory effect on ERK-1/2 pathway although siRNA targeting PKCε or PKCζ decreased it. If more specific inhibitor is developed in future, it would be more useful.

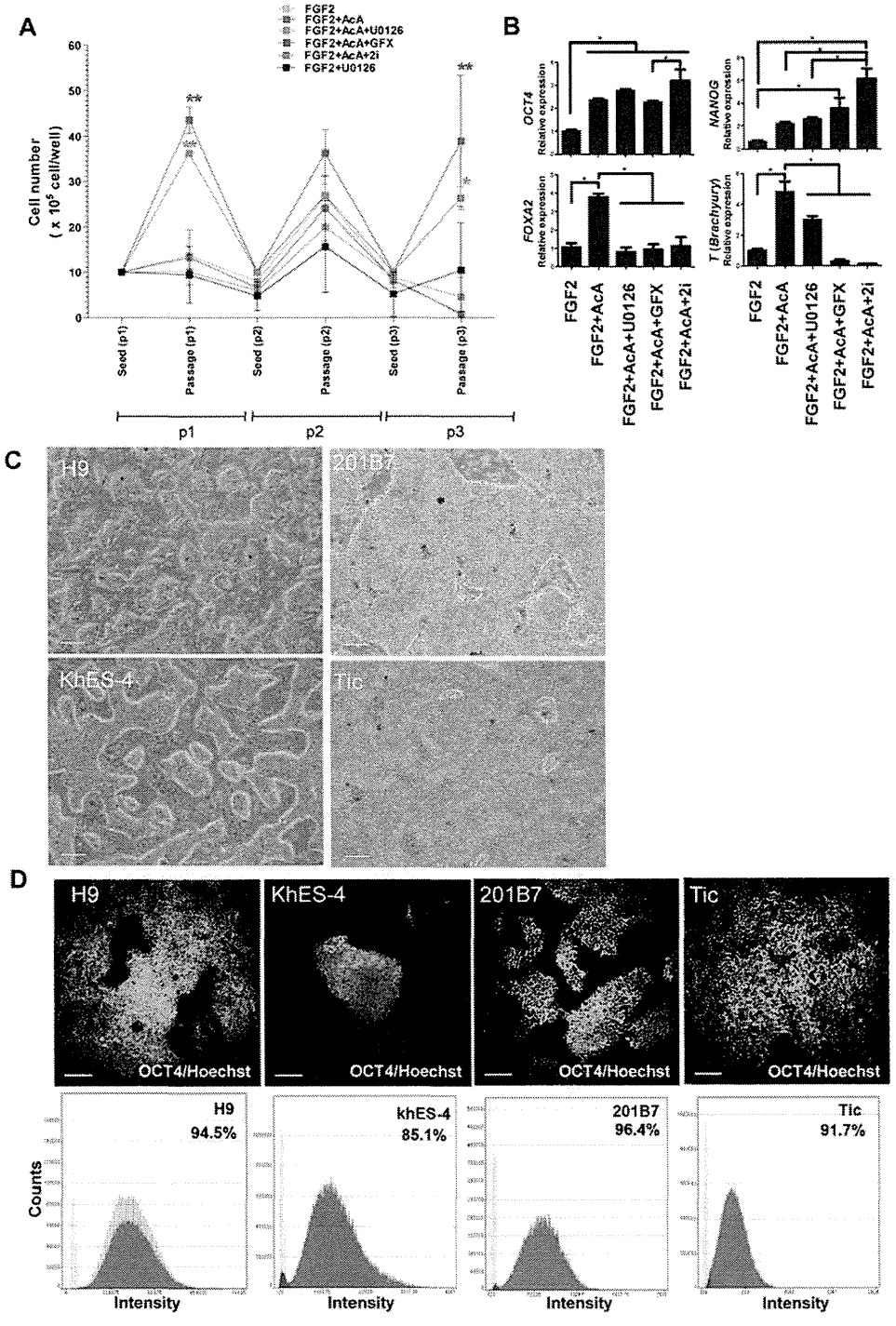

Figure 5. Single cell culture of hPS cells in the hESF9a$_{2i}$ medium. (A) Cell growth of dissociated single H9 hES cells cultured in each indicated condition for three passages. Cells were reseeded at the cell density of 1×10^6 cells/well every 5 days. When the cells were passages, cell numbers were counted. Cell growth in the hESF9a$_{2i}$ medium was significantly different ($P<0.05$) from hESF9 (FGF-2), FGF-2 + activin A, FGF-2 + activin A + U0126. Cell growth in hESF9a + GFX was significantly different ($P<0.05$) from hESF9 (FGF-2), FGF-2 + activin A, FGF-2 + activin A + U0126, and FGF2 + U0126. The data are represented as means ± SE (n = 3). (**B**) Gene expression in the hPS cells cultured in each indicated condition for three passages. The gene expression levels of NANOG, OCT3/4, FOXA2, T in the cells were measured by real-time RT-PCR. On the y axis, the gene expression level in the cells cultured with FGF-2 in a experiment was taken as 1.0. The data are represented as means ± SE (n = 3). *$P<0.05$. (**C**) Phase-contrast image of hPS cells grown on FN in hESF9a$_{2i}$ medium for 3 passages. The cells were dissociated into single cells for passage, and reseeded at a ratio of 1:3 - 1:5 every five days. Scale bars, 200 μm. (**D**) OCT3/4 expression in hPS cells grown on FN in hESF9a$_{2i}$. The cells grown in hESF9a$_{2i}$ as described above in Figure 5C were reseeded on a 6-well-plate and cultured for 5 days. The cells stained with anti-OCT3/4 antibody were visualized with Alexa Fluor 488 (upper panels). Nuclei were stained with Hoechst 33342 (blue). Scale bars, 200 μm. Whole cell images in whole plate were captured and OCT3/4 expression profiles were analyzed by Image Analyzer (lower panels). Antigen histogram (red); control histogram (green); Y axis is cell numbers and X axis is fluorescence intensity for anti-OCT3/4 antibody.

doi:10.1371/journal.pone.0054122.g005

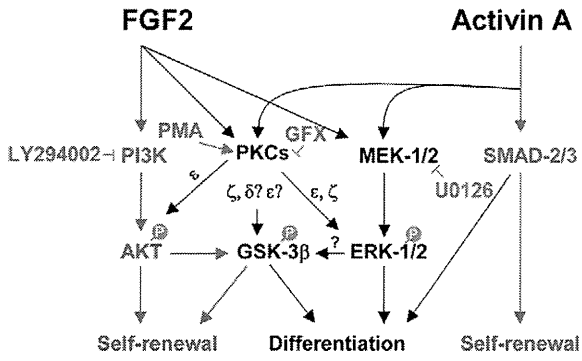

Figure 6. Model for the molecular mechanism of PKCs regulating self-renewal or differentiation in hPS cells. Our study suggested a model that FGF-2 activates PI3K/AKT, MEK/ERK-1/2, and PKCε/δ/ζ. PKCε, δ, and ζ inactivates directly or indirectly GSK-3β by phosphorylation which promotes differentiation of hPS cells. PKCε and ζ activates ERK-1/2 which promotes differentiation of hPS cells. Activin A activates SMAD-2/3 which controls self-renewal and differentiation while activin A together with FGF-2 activates both ERK-1/2 and PKCs. Inhibition of both ERK-1/2 and PKCs pathway provides a metastable undifferentiated state of hPS cells. Blue arrow indicated pathway promoting hPS cell self-renewal and black arrow indicated pathway promoting hPS cell differentiation.
doi:10.1371/journal.pone.0054122.g006

To maintain undifferentiated state, balancing among ERK-1/2, PI3K, SMAD, and PKC signal pathways may be required in any culture conditions. KSR of which components are not disclosed in public is known to have BMP-4-like activity [55]. Some components including BMP-4 in KSR together with secreting factors from mouse feeders might regulate PKC/ERK-1/2 signaling. Using our defined conditions, more molecules including growth factors would be screened to detect their accurate effects on hPS cells.

In conclusion, our study suggested that FGF-2 induced PI3K/AKT and MEK/ERK-1/2, but also PKCs in hPS cells. PI3K/AKT promotes cell self-renewal whereas the MEK/ERK-1/2, PKC/ERK-1/2 and PKC/GSK-3β pathways down-regulate hPS cell self-renewal. This study helps to untangle the cross-talk between molecular mechanisms regulating self-renewal and differentiation of hPS cells.

Materials and Methods

Chemicals

A chemical library of kinase inhibitors (Biomol, Plymouth Meeting, PA, USA), LY-294002 (Cell Signaling Technology, Beverly, MA, USA), BIO (Merck, Darmstadt, Germany), U0126 (Promega, Madison, WI, USA), Y-27632 (Wako Pure Chemical, Osaka, Japan), PMA (Sigma, St. Louis, MO, USA), 4α-PMA (Promega) and Gö6976 (Sigma) were dissolved in dimethyl sulfoxide (DMSO). LiCl (Sigma) and GF109203X hydrochloride (Sigma) were dissolved in water.

PKC inhibitory peptides

Membrane-permeable PKCδ inhibitory peptide δV1-1 (SFNSYELGSL: amino acids 8-17 of PKCδ) or PKCε inhibitory peptide εV1-2 (EAVSLKPT: amino acids 14-21 of PKCε) were designed according to the method of Mochly-Rosen [56–57]. The peptides were custom-synthesized by Sigma (purified to >95% by HPLC). Myristoylated PKCα, β, and γ inhibitory peptide and myristoylated PKCζ inhibitory peptide were purchased from Promega and Calbiochem (Darmstadt, Germany), respectively.

Cell culture

The hES cell lines, H9 [10,31] (WA09, WISC Bank, WiCell Research Institute, Madison, WI, USA) and KhES-4 (provided by Kyoto University, Kyoto, Japan), and hiPS cell lines, 201B7 [26] (provided by Dr. Shinya Yamanaka, Kyoto University) and Tic (JCRB1331, JCRB Cell Bank, Osaka, Japan) [33,58] were routinely maintained on mitomycin C-inactivated mouse embryo fibroblast feeder cells (MEF, Millipore Co., Billerica, MA, USA) in an KSR-based medium supplemented with 5 ng/ml (H9, khES-4), 4 ng/ml (201B7) or 10 ng/ml (Tic) human recombinant FGF-2 (Katayama Kagaku Kogyo LTD., Osaka, Japan) previously described [10]. Human ES cells were used following the Guidelines for utilization of human embryonic stem cells of the Ministry of Education, Culture, Sports, Science and Technology of Japan after approval by the institutional ethical review board at National Institute of Biomedical Innovation. The cells were passaged with 1 mg/ml dispase (Roche, Mannheim, Germany) in DMEM/F12 medium and a plastic scraper (Sumitomo Bakelite Co., LTD Tokyo, Japan). The cells were split at a ratio of 1:5–1:8 every 5 days.

Human ES/iPS cell culture in feeder-free and growth factor defined serum-free medium

Prior to culture in feeder-free conditions, the medium was changed from the KSR-based medium to a growth factor-defined serum-free hESF9 medium [8] (Table S1). Two days after the medium change, the cells were harvested with 1 mg/ml dispase or TrypLE (Invitrogen), and reseeded on plastic plates coated with bovine FN (Sigma, 2 μg/cm^2) [21]. For long-term culture, hPS cells were maintained on FN in hESF9 medium supplemented with 10 ng/ml human recombinant activin A (R&D Systems Minneapolis, MN, USA) in the presence of both 5 μM U0126 [20], and 5 μM GFX, designated hESF9a$_{2i}$ medium. The medium was changed every day.

Single hPS cell culturing with two inhibitors

hPS cells were dissociated with TrypLE (Invitrogen) into single cells, and seeded on a 6-well plate coated with FN at the cell density of 1×10^6 cells/well in hESF9, or supplemented with 10 ng/ml activin A, 5 μM U0126, or 5 μM GFX. The medium was changed every day.

Quantitative ALP activity-based high-throughput screening assay

The hPS cells were dissociated with accutase into single cells and seeded at 5×10^4 cells/well on a 96-well plate coated with FN (FN, 2 μg/cm^2) in hESF9 medium. Each compound in the chemical library was added at 2.5 μM to each well. After further 5 days-culture, the cells were washed with 3-[4-(2-Hydroxyethyl)-1-piperazinyl] propanesulfonic acid (EPPA) buffer (30 mM, pH 8.2). Fluorescence ALP substrate (0.2 mM, 4-methylumbelliferyl phosphate) [59] in EPPS buffer was added into the wells. After incubation for 30 min at 37°C, EPPS buffer (100 mM, pH 7.7) supplemented with 1 M K_2HPO_4 was add to terminate the enzyme reaction. The amount of 4-methylumbelliferone (4-MeU) produced via the enzyme reaction was measured with a fluorescence microplate reader (Gemini EM, Molecular Devices, Menlo Park, CA). The specific activity of ALP was quantified by reference to a standard fluorescence curve generated with known concentrations of 4-MeU (Sigma).

Colony formation assay

Dissociated single hPS cells were seeded at 10,000–250,000 cells/well on a 6-well plate coated with FN (2 μg/cm^2) in hESF9 medium supplemented with and without 1 μM GFX. After 5-days-culture, the colonies were fixed in 4.5 mM citric acid, 2.25 mM sodium citrate, 3.0 mM sodium chloride, 65% methanol, and 3% formaldehyde for 5 min, and stained with ALP fast-red substrate (Sigma) for 15 min at room temperature.

Immunocytochemistry

Immunocytochemistry was performed as described previously [20,60]. The image analysis was performed with In Cell analyzer 2000 and Developer tool box software (GE Healthcare, Little Chalfont, Buckinghamshire, UK), or a confocal microscope (Carl Zeiss). The primary and secondary antibodies used were listed in Table S2.

Western blotting

Western blots were performed as described previously [8,20,60]. Protein (2 μg/lane) was separated by 12.5% SDS-PAGE and transferred to polyvinylidene fluoride (PVDF) membranes (Millipore). The membranes were reacted with primary antibodies, peroxidase-conjugated secondary antibodies, and ECL Plus reagent (GE Healthcare). Protein bands were visualized using LAS-4000 imager (Fujifilm, Tokyo, Japan). The primary antibodies used were listed in Table S2.

AlphaScreen assay

AlphaScreen® SureFire® Cell-based Assay (Perkin-Elmer, Waltham, MA, USA) was performed to measure phosphorylation of AKT-1/2/3, ERK-1/2, and GSK-3β in the cells according to the manufacturer's instructions. Materials used were listed in Table S2. The fluorescence signal was measured using an EnSpire™ plate reader (PerkinElmer).

Gene expression analysis

Total RNA extracted from cultured cells using RNeasy Mini kit (Qiagen, Valencia, CA, USA) were treated with DNase I to remove any genomic contamination, and reverse-transcribed using Superscript VILO cDNA synthesis kit (Invitrogen) according to the manufacturer's instructions. For RT-PCR, PCR products were amplified with AmpliTaq Gold DNA polymerase (Applied Biosystems, Foster City, CA, USA), following manufacturer's instruction. The DNA was separated by gel electrophoresis and visualized under ultraviolet light for photography. For quantitative real-time RT-PCR, PCR was performed based on the TaqMan or the SYBR Green gene expression technology in a 7300 Real Time PCR System (Applied Biosystems), following manufacturer's instruction. Threshold cycles were normalized to the housekeeping gene GAPDH and translated to relative values. Specific primers used are listed in Tables S3 and S4. For PCR-array, TaqMan low-density human stem cell pluripotency card PCR array (Applied Biosystems, Foster City, CA) was performed as previously described [61]. Expression levels were all normalized against the housekeeping gene β-actin. The relative expression levels of each gene in embryoid bodies were compared to the levels in H9 hES cells or 201B7 hiPS cells grown on feeders in KSR-based medium.

Transfections with siRNA

Transfections with siRNA were performed using Dharmafect1 (Dharmacon, Chicago, USA) as previously described [62]. Prior to transfection, the hiPS cells were incubated with ROCK inhibitor Y-27632 (10 μM) for 1 hour and dissociated with TrypLE (Invitrogen) and pelleted by centrifugation. To prepare siRNA/lipid solutions, 50 pmol of siRNAs were diluted in 100 μl of hESF9 medium. In a separate tube, 6 μl of Dharmafect1 was diluted in 100 μl of hESF9 medium. The solution of the two tubes were mixed and incubated at room temperature for 20 mins. The resulting 200 μl of siRNA/lipid solution in hESF9 medium was used to resuspend the cell pelleted containing from 1×10^4 to 1×10^5 cells, and suspension incubated at room temperature for 10 min. After incubation, 1.5 ml of prewarmed hESF9 medium containing ROCK inhibitor (10 μM) was added and the suspension transferred into a FN-coated well of 24-well or 6-well plate, followed by culture for 24 hour. After recovery in fresh hESF9 medium, cells were transfected again at 24 hours. Total RNAs or proteins were extracted for analysis 72 hours after the fast transfection. siRNAs were listed as Table S4.

Live cell imaging analysis

After seeded on a 6-well plate coated with FN, the cells were incubated in a live cell imaging system, BioStation CT (Nikon Instruments Inc., Tokyo, Japan) at 37°C 10% CO_2. The images were captured every 12 hours and analyzed by a soft ware CL-Quant (Nikon Instruments Inc.).

Cell Growth

The cells were inoculated on a 6-well plate coated with FN at the cell density of 250,000 cells/well in hESF9 medium including 10 ng/ml FGF-2, supplemented with 0.1% DMSO, GFX in H_2O, or Gö6976 in DMSO. After 5 days culture, the cell numbers were counted by Coulter Counter (Beckman Coulter, Inc).

Flow cytometry

Flow cytometry was performed as described previously [61] with a FACS Canto flow cytometer (BD Biosciences). The primary antibodies used were listed in Table S2.

In vitro cell differentiation

In vitro differentiation was induced by the formation of embryoid bodies as described previously [61]. Floating embryoid bodies were maintained in DMEM with 10% FCS for more 14 days.

Teratoma formation

The cells were harvested by dispase treatment, collected into tubes, and centrifuged, and the pellets were suspended in DMEM supplemented ROCK inhibitor. The cells from a confluent one-well in 6-well plate were injected to the rear leg muscle or thigh muscle of a SCID (C.B-17/lcr-scid/scidJcl) mouse (CLEA japan, Tokyo, Japan). Nine weeks after injection, tumors were dissected, weighted, and fixed with 10% formaldehyde Neutral Buffer Solution (Nacalai tesque, Kyoto, Japan). Paraffin-embedded tissue was sliced and stained with hematoxylin and eosin. All animal experiments were conducted in accordance with the guidelines for animal experiments of the National Institute of Biomedical Innovation, Osaka, Japan.

Karyotype analysis

Log phase hPS cells (day 3–4 after subculture) were treated with metaphase arresting solution (Genial Genetic Solutions Ltd., Cheshire, UK) for 5 hr. The treated hPS cells were collected with 0.1% EDTA and processed according to the quality control protocol in the JCRB Cell Bank (http://cellbank.nibio.go.jp/cellbank.html). Chromosome numbers were counted in 20

metaphases, and G-banding karyotype analysis was performed on 20 metaphase cells per sample.

Supporting Information

Figure S1 The phosphorylation of AKT, GSK-3β, and ERK-1/2 was confirmed by western blot analysis using an antibody to AKT, GSK-3β, and ERK-1/2 and their phosphorylated forms. Each gel image is a representative of independent three to five experiments. (**A**) Time course of phosphorylation level of AKT, GSK-3β, and ERK-1/2. H9 hES cells were stimulated with FGF-2 (100 ng/ml) with or without GFX (5 μM) for 180 minutes after overnight starvation of FGF-2 and insulin. (**B**) Effect of inhibitors on phosphorylation level of AKT, GSK-3β, and ERK-1/2. After starvation of FGF-2 and insulin overnight, 201B7 hiPS cells were stimulated with FGF-2 (100 ng/ml) for 15 min with LY294002, GFX, U0126, or BIO or without GFX (5 μM). (**C**) Effect of BMP-4 or activin A on phosphorylation level of AKT, GSK-3β, and ERK-1/2. After starvation of FGF-2 and insulin overnight, 201B7 hiPS cells were stimulated with with FGF-2 (100 ng/ml), BMP-4 (10 ng/ml) or activin A (100 ng/ml). (**D**) Effect of addition of activin A with and without inhibitors on phosphorylation level of AKT, GSK-3β, and ERK-1/2. After starvation of FGF-2 and insulin overnight, H9 hES cells were stimulated with FGF-2 (10 ng/ml) and activin A (10 or 100 ng/ml) together with U0126 (5 μM) and GFX (5 μM) or Gö6976 (5 μM) for 15 minutes. (**E**) Effect of GFX concentration on phosphorylation level of AKT, GSK-3β, and ERK-1/2. After starvation of FGF-2 and insulin overnight, H9 hES cells were stimulated with FGF-2 (100 ng/ml) with GFX at 1~10 μM. The phosphorylation levels in the cells were measured by AlphaScreen® SureFire® assay kit. The values of the y-axis are the ratio of each phosphorylation to each total signal protein. The data are represented as means ± SD (n = 3). *P<0.05.
(TIF)

Figure S2 Summary of the result of the effect of PI3K, MEK-1/2, or PKCs inhibitor on FGF-2-induced phosphorylation of AKT, GSK-3β, and ERK-1/2.
(TIF)

Figure S3 Knockdown efficacy and effect of siRNA targeting PKCδ, ε, and ζ. (**A**) Total RNAs were extracted for analysis 72 hours after the fast transfected to 201B7 iPS cells. The efficacy of siRNA was evaluated by quantitative RT-PCR. siRNAs and primers were listed as Table S4. (**B**) Summary of the result of the PKCδ-, PKCε-, PKCζ-knockdown effect on phosphorylation of GSK-3β and AKT in FGF-2 signaling.
(TIF)

Figure S4 Effect of inhibitory peptides for PKCs on phosphorylation level of ERK-1/2. After starvation of FGF-2 and insulin, the H9 hES cells (right panel) or the 201B7 iPS cells (left panel) were stimulated with FGF-2 (100 ng/ml) for 15 mins with indicated combination of membrane-permeable specific inhibitory peptides for PKC isoforms; PKCα, β, and γ inhibitory peptide (50 μM), PKCδ inhibitory peptide (50 μM), PKCε inhibitory peptide (50 μM), or PKCζ inhibitory peptide (20 μM). The phosphorylation levels in the cells were measured by AlphaScreen® SureFire® assay kit. The values of the y-axis are the ratio of each phosphorylation to each total signal protein. The data are represented as means ± SD (n = 3). *P<0.05.
(TIF)

Figure S5 Culture of hiPS cells in the hESF9 + activin A + 2i or the hESF9 + activin A + GFX conditions. (**A**) Phase-contrast image of H9 hES cells serially cultured in hESF9 + activin A + 2i (hESF9a_{2i}) or hESF9 + activin A + GFX mediums at three passages, as described in Figure 5A and 5B. Scale bars, 200 μm. (**B**) Immunocytochemical staining for OCT3/4 expression of H9 cells cultured as described (A). The H9 hES cells stained with anti-OCT3/4 antibody were visualized with Alexa Fluor 488 (green). Nuclei were stained with Hoechst 33342 (blue). Scale bars, 50 μm. (**C**) Anti-OCT3/4 staining intensity profiles in the cell population grown in the hESF9 + activin A + 2i or the hESF9 + activin A + GFX conditions were analyzed by IN Cell image analyzer (lower panels). Antigen histogram (red); control histogram (green); Y axis is cell numbers and X axis is fluorescence intensity for anti-OCT3/4 antibody.
(TIF)

Figure S6 Immunocytochemical staining of H9, KhES-4, 201B7, and Tic hPS cells for TRA-1-60. The cells grown on FN in hESF9a_{2i} as described in Figure 5C were stained with TRA-1-60 antibody and Alexa Fluor 647-conjugated secondary antibody. Nuclei were stained with Hoechst 33342 (blue). Scale bars, 200 μm.
(TIF)

Figure S7 Long-term culture of hiPS cells in the hESF9a_{2i} medium. Human iPS 201B7 cells were cultured on FN in hESF9a_{2i} medium serially for more than 30 passages. The cells were split at a ratio of 1:3–1:5 every five days. (**A**) Phase-contrast image of 201B7 hiPS cells cultured on FN in hESF9a_{2i} medium. (**B**) A comparison of the growth of 201B7 cells in hESF9a_{2i} medium or KSR-based media. The cells were seeded on feeders in KSR-based medium (closed circles) or on FN in hESF9a_{2i} medium (open circles; mean + s.d. of three experiments. Cell numbers were counted every 2 days. (**C**) Immunocytochemical staining for SSEA-1, SSEA-4, TRA-1-60 and TRA-1-81 (red) expression of 201B7 cells (passage 10) cultured on FN in hESF9a_{2i}. Nuclei were stained with Hoechst 33342 (blue). Scale bars, 200 μm. (**D**) FACS profiles for SSEA-1, SSEA-4, TRA-1-60, TRA-1-81, TRA-2-54, A2B5, CD90, and HLA-Class1 expression of hiPS 201B7 cells (passage 22) cultured on FN in hESF9a_{2i} medium. Antigen histogram (red); control histogram (green); the horizontal bar indicates the gating used to score the percentage of antigen-positive cells.
(TIF)

Figure S8 Long-term culture of hES cells in the hESF9a_{2i} medium. Human ES H9 cells were cultured on FN in hESF9a_{2i} medium serially for more than 30 passages. The cells were split at a ratio of 1:3–1:5 every five days. (**A**) Phase-contrast image of H9 hES cells cultured on FN in hESF9a_{2i} medium. (**B**) A comparison of the growth of H9 hES cells (passage 13, 16, and 17) in hESF9a_{2i} (open circles) or KSR-based media (closed circles). Mean + s.d. of three experiments. (**C**) Immunocytochemical staining for SSEA-1, SSEA-4, TRA-1-60, TRA-1-81, TRA-2-54, A2B5, CD90, and HLA-Class1 expression (red) in H9 hES cells (passage 13). Nuclei were stained with Hoechst 33342 (blue). (**D**) FACS profiles of H9 hES cells (passage 14). Antigen histogram (red); control histogram (green). Scale bars = 200 μm.
(TIF)

Figure S9 Karyotype analysis and differentiation potential of H9 hES cells and 201B7 hiPS cells maintained in hESF9a_{2i} conditions. (**A**) Karyotype analysis of H9 hES cells at passage 15 and 201B7 hiPS cells at passage 21, showing a normal diploid 46, xx karyotype. (**B**) Heat-map of gene expression in H9 hES cells (at passage 10–13) and 201B7 hiPS cells (at passage 10–20) those during in vitro differentiation in triplicate experiments (Sample No. 3–5). TaqMan low density PCR arrays